COMPUTER AIDED ANALYSES OF SMOKE STACK DESIGNS

by

Joseph Charles Servaites

Thesis submitted to the Faculty of the
Virginia Polytechnic Institute and State University
in partial fulfillment of the requirement for the degree of

MASTER OF SCIENCE
in
MECHANICAL ENGINEERING

APPROVED:

_____

Dr. Larry D. Mitchell, Chairman

_____ _____

Dr. Clint L. Dancey Dr. Reginald G. Mitchiner

September, 1996

Blacksburg, Virginia

Keywords: Stack, Transfer Matrix, Vibration, Tapered Beam, Vortex Shedding

COMPUTER AIDED ANALYSES OF SMOKE STACK DESIGNS

by

Joseph Charles Servaites

Dr. Larry D. Mitchell, Chairman

Department of Mechanical Engineering

The purpose of this research is to analyze the statics and dynamics of steel smoke stacks subject to excitation by aerodynamic forces. The wind loads experienced by smoke stacks arise from various phenomenon, the most prominent of which are static drag load, vortex shedding, and atmospheric turbulence. The nature of these loading sources around a cylinder are studied in detail. Both static and dynamic loads are capable of producing large tip deflections, and are of the most prominent design criteria for stack designers. A computer program, STACK1, has been created by modifying an existing analysis code, BEAM8, to be used specifically for stack analysis. This analysis code utilizes the transfer matrix method to perform detailed bending and vibration analyses. This new software has been developed to check stack designs for compliance with appropriate steel stack standards, and provide the designer with information regarding the static and dynamic response of the structure. A detailed analysis is performed to demonstrate the validity of approximating a tapered Timoshenko beam with a series of continuous, constant cross-section beams.

Acknowledgment

The author would like to express sincere gratitude to his major advisor, Dr. Larry D. Mitchell, for the immense amount of support, patience, and guidance provided for this thesis and research. The author is also obliged to committee members Prof. Clint L. Dancey and Prof. R. G. Mitchiner for providing advice and for reviewing the thesis.

The author would also like to thank the DuPont Company for its development and sponsorship of this project. Specifically, the author thanks Dr. K. John Young and Dr. Jimmy Y. Yeung without whose suggestions and support this research could not have been completed.

Table of Contents

Aerodynamic Forces on Stacks

Transfer Matrix Method

BEAM8 Modifications and Implementation of ASME and ASCE Standards to Generate STACK1

Test Examples

Conclusion and Recommendations

List of Illustrations

Chapter 1: Introduction

1.1 Definition

The purpose of this research is to analyze steel smoke stacks subject to excitation by aerodynamic forces. The loads experienced by smoke stacks arise from various phenomenon, the most prominent of which are static drag load, vortex shedding, and atmospheric turbulence. These sources are capable of producing large tip deflections, and are of the most prominent design criteria for stack designers. A computer program, STACK1 has been created by modifying an existing analysis code, BEAM8, to be used specifically for stack analysis. This new software has been developed to check stack designs for compliance with appropriate steel stack standards and provide the designer with information regarding the static and dynamic behavior of the structure.

1.2 Application of Research

The results of this research will help smoke-stack designers by providing insight into the nature of wind and stack interactions. The designer will be able to expedite the design process by using the computer program STACK1. This program is intended to be completely self contained, that is, a complete analysis can be performed with a single executable file. The STACK1 program is designed to perform an analysis of a smoke stack design, then compare the static and dynamic behavior of the design with existing

standards. Any inconsistencies between the given design and the standards are brought to the user's attention.

1.3 Existing Suppression Mechanisms

The dynamic control of stacks is a complex problem. Many methods already exist to suppress vibrations, including helical strakes, shrouds, and variation of structural parameters such as wall thickness and diameter. Figure 1-1 shows various suppression devices which are designed to alter the flow field around the cylinder to prevent periodic vortex shedding.

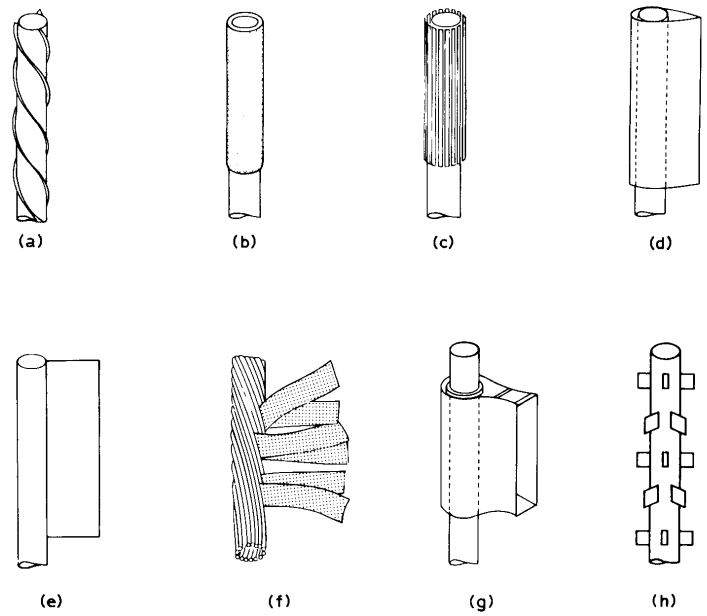

Figure 1-1. Add-on devices for suppression of vortex-induced vibration of cylinders, after Blevins [1]

Because steel stacks have very little inherent structural damping, vibrations can be further suppressed by increasing the stack damping. Methods for increasing the damping include mass dampers, foundation fabric pads, hanging chains, and other devices [2].

It is of interest to design a stack with inherent dynamic stability. If a stack could be designed to minimize deflections and avoid resonances, then fewer "add-on" suppressions mechanisms would be necessary, and therefore reduce the cost, weight, and complexity of the stack.

1.4 Aerodynamic Forces on Stacks

Two basic types of loads can be applied by wind: static pressure and harmonic excitation. These loads are normally experienced simultaneously, although static drag can exist without harmonic excitation under certain conditions [3]. Smoke-stack designers have devised many methods to control the static and dynamic behavior of stacks. The static deflection can be reduced increasing the stiffness of the stack or by modifying the air flow field in the vicinity of the stack to reduce the drag load. The overall stiffness of the stack can be enhanced by geometric modifications, such as increasing the wall thickness or increasing the stack diameter. Guy wires can be added to enhance structural stiffness and raise the resonance frequencies. Methods of modifying the air-flow field around a single stack include changing the stack diameter, and attaching external devices to the stack, such

as plates, shrouds or helical strakes. If multiple stacks are present, certain spatial arrangement patterns can help reduce the static wind loads.

1.5 Analysis Methods

In order to analyze stack designs, beam bending and vibration theory is used. Various methods exist for analyzing beams, such as the so-called continuum method, the finite element method, and the transfer matrix method. In the continuum method, the beam is considered a continuous structure. Differential equations have been developed to represent beams in the continuum, and these equations are solved by standard methods. The arbitrary constants in the equations are determined by the boundary conditions of the problem.

The finite element method, however, considers the beam to be broken up into a series of small elements connected at adjacent nodes. The elastic behavior of the beam is then found by calculating the relationship between force and displacement at each node. Equilibrium and compatibility conditions at each node can be determined from the elastic behavior, and an overall stiffness matrix is found in terms of unknown nodal displacements. Nodal displacements are calculated by inverting the stiffness matrix, and these displacements can be used to determine the stress in the beam.

The premise of the third method, the transfer matrix method, is that a complex structure can be broken up into a series of simple structures. The properties of each section are expressed in matrix form. Because the transfer matrix method uses continuum solutions to describe each component of the structure, displacements and internal forces can be found at any point along the structure. These displacements include deflection (w) and angle (ψ), and the internal forces include moment (M) and shear (V). These are arranged in a state vector, which describes the "state" of deflection and internal loading of the structure. The state vectors on either side of a section are related by the transfer matrix of the section. The matrix across the length of a section is called a *field* transfer matrix, and the matrix across a point parameter such as a point mass, point load or point moment, is called a *point* transfer matrix. A complex beam can be modeled as a series of field and point transfer matrices. In order to relate the state vector at one end of the structure to the other end, the intermediate transfer matrices are successively multiplied.

Each method described has inherent advantages and disadvantages. The classical continuum method is useful for only very simple structures, and quickly becomes cumbersome for more complex structures. The finite element method can provide very accurate results if sufficient detail is included in the model, but the model building process can be time consuming, the computational efforts are time consuming, and very large computer resources are required to handle the size of the stiffness matrix. The size of

these matrix operations depend on the number of degrees of freedom used in the model. The transfer matrix method, on the other hand, is very simple, and extremely useful for structures that have a non-branching shape, that is, the structure can be modeled as a series of elements linked together end-to-end in a linear topology. Various loading configurations are easily modeled, including constant pressure or linearly varying pressure. This method is not as useful for branched or coupled systems.

Smoke-stack geometry usually consists of various elements connected end-to-end. The properties of stack sections are easily expressed in matrix form by using the differential equation for a beam. Wind loads on a stack can be approximated as linearly varying pressures along each section. It is for these reasons that the transfer matrix method is very well suited for stack analysis.

Chapter 2: Literature Survey

2.1 Smoke-Stack Concerns

The purpose of a smoke stack is to vent exhaust gasses to the atmosphere [4]. The mechanical design of smoke stacks is controlled in part by air pollution rules and regulations. Stack heights and diameters are set by a considering both structural behavior and function, while simultaneously meeting the requirements for air pollution control. In years of late, the height requirements for stacks have increased to satisfy air pollution regulations [4]. The design and analysis of smoke stacks are complex problems. Because of the particular nature of stacks and their susceptibility to failures due to wind and seismic-induced vibrations, along with corrosion and erosion, the design process is very complex [5]. In addition to these structural concerns, recent regulations by the Environmental Protection Agency (EPA) concerning emissions have placed a strong emphasis on the mechanical design of stacks [5].

2.2 Steel Smoke-Stack Standards

In April of 1979 a group comprised of stack users, researchers, designers, fabricators, and erectors all met to formulate a building code. The results of this meeting is a set of comprehensive guidelines for mechanical design, material selection, the use of linings and coatings, structural design, vibration considerations, access and safety, electrical requirements, and fabrication and construction of steel stacks. These standards were

compiled and approved as an American National Standards Institute (ANSI) Standard in August, 1986 and published as ASME/ANSI STS-1-1986 in May 1988 [2]. Much of the procedures outlined within the ASME standards have been adapted by the American Society of Civil Engineers (ASCE). The ASCE Steel Stack Standards [6], revised in 7-95, provide essentially the same concepts as the ASME standards, with several modifications.

2.3 Stack Analysis and Aerodynamic Interactions

In 1987 the ASCE compiled a text concerning wind loading and wind-induced structural response [7]. This text supplements the ASCE standards by providing detailed information on the wind environment, fundamentals of aeroelasticity, design concerns of low buildings, tall buildings, and stacks. This text points out that the design of stacks must take into consideration the effects of both along-wind and across-wind loads [8]. The text then proceeds to provide two methods to find the peak response of a stack.

In 1990 the Department of Civil Engineering at the University of Roorkee, India published the *Proceedings of the International Symposium of Experimental Determination of Wind Loads on Civil Engineering Structures* [9] [10]. This proceedings also included a detailed analysis of the wind environment [9], as well as design considerations for buildings and smoke stacks. In the paper dealing with wind loads on stacks, Vickery [10]

provides in-depth discussions of various excitation sources, including forces induced by turbulence, wake effects, and motion-induced forces. Perhaps the most significant information provided is that regarding aerodynamic damping. He describes how aerodynamic damping can adversely affect structural vibrations. Aerodynamic damping is almost always positive in the along-wind direction, but is very commonly negative in the across-wind direction, thus leading to a severely underdamped structure. He shows that negative aerodynamic damping in the across wind vibration may well be of the same order as the positive structural damping. If the negative aerodynamic damping exceeds the internal structural damping the net damping goes negative. The problem converts from a vibration response problem to a dynamic stability problem.

A more detailed look at the fluid mechanics involved with flow over a cylinder is provided by Blevins [11]. He provides a detailed description of the flow field around a cylinder, as well an explanation of how the drag and lift forces originate. He also describes in detail how the flow field changes with respect to a dimensionless parameter called the *Reynolds number* (*Re*).

2.4 Transfer Matrix Method

As mentioned previously, the transfer matrix method is an ideal method of analysis for smoke stacks. The necessary transfer matrix theory to perform detailed beam bending and vibration analyses is provided by Pestel and Leckie [12]. The theory behind transfer

matrix analysis as it applies to static and dynamic analyses is developed in detail. A wide variety of transfer matrices are presented in, including those for forced vibration. Various examples are provided throughout the text to supplement the theory. Transfer matrices for tapered beams including shear deformation and rotary inertia are not provided, however.

In 1995 Shen [13] published a journal article dealing with the use of transfer matrices to analyze tapered timoshenko beams. This article, however, does not derive a transfer matrix for a continuously tapered beam, rather, it deals with approximating a tapered beam with a series of continuous beam segments. The rate of convergence of a transfer matrix model is compared to that of a finite element model, and it is shown that the transfer matrix model converges much faster.

Chapter 3: Aerodynamic Forces on Stacks

3.1 Introduction

All buildings and stacks are subjected to various types of aerodynamic loading. Static drag forces can cause a structure to deflect significantly, especially in intense storms. A wind-bearing structure must be designed to withstand the stresses imposed by these static loads. The presence of dynamic loading on structures does not require extremely high wind velocities, only that one or more harmonic excitation sources be present. These dynamic loads, if acting at or near a structural resonance, can cause large vibration amplitudes. A structure subjected to dynamic loading must be able to withstand not only the maximum stresses induced by large deflections, but must also be resistant to fatigue failure. The first step in correctly designing a wind-bearing structure is to understand the applied loading.

3.2 Sources of Aerodynamic Loads

The sources of stack excitation investigated in this study are limited to aerodynamic loads. Wind across a structure gives rise to a variety of static and dynamic forces, in both the along-wind and cross-wind direction. The aerodynamics associated with a smoke stack is very similar to that of tall buildings from a general point of view. There are several aspects, however, that allow various differences in stack analysis and design.

Buildings generally posses a much lower aspect ratio (height/width) than stacks. Buildings are typically located in cities, where surrounding buildings of comparable height are present. The airflow over buildings is, therefore, strongly three dimensional, and very dependent on the surrounding structures [10]. However, most stacks are very tall, slender structures, with very large aspect ratios. Stacks typically rise well above the surrounding buildings and, therefore, are not subject to large amounts of interference effects. The majority of the airflow over a stack is approximately two-dimensional, and this assumption will be used to calculate the forces induced by wind. Another important difference between buildings and stacks involves the design criteria. Tall buildings must be designed so that accelerations (swaying) are kept to a minimum. The design of stacks, however, is normally limited by material strength only.

In order to correctly design stacks one must consider both the static and dynamic response.

3.3 Static Response, Associated Stresses, Deflections.

Perhaps the most obvious design concern in stacks is static deflection. Significant static wind loads can develop in windy conditions, especially in coastal regions where wind speeds can exceed 110 mph (49 m/s) [14]. One should bear in mind the substantial wind velocity gradient near the earth's surface. This gradient is due to what is called the

atmospheric boundary layer, which extends approximately 1000 m (3281 ft) above the earth, as shown in Figure 3-1.

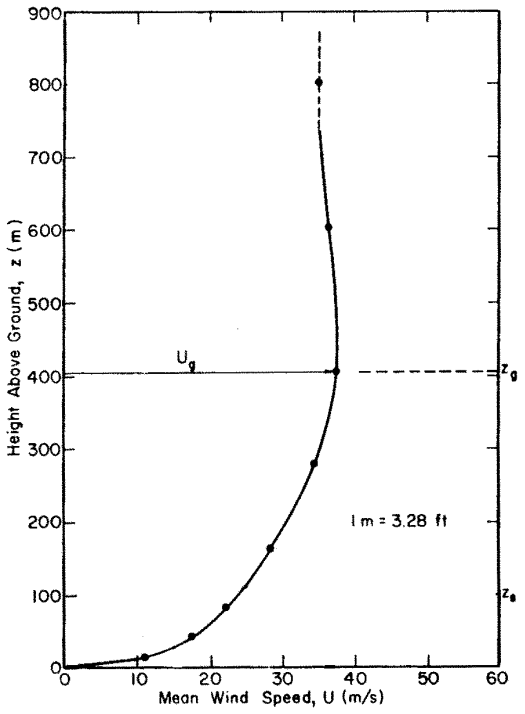

Figure 3-1. Example of Planetary Boundary Layer Velocity Profile, after Cermak [16]

From Figure 3-1, it is apparent that for extremely tall structures the tip wind velocity can be much greater than for shorter structures. Flow above the wind-gradient level z_g is mainly influenced by horizontal temperature gradients, while flow below this level is mainly influenced by surface topography [16]. The shape of this velocity profile is

dependent on a number of variables, including surface roughness, temperature gradients, pressure gradients, and upper atmospheric conditions. It is assumed that the static forces generated by the wind depend on the velocity of the wind relative to the structure. These forces can be represented by a drag force *D* in the along wind direction and a lift force *F* in the across wind direction. The static drag force *D* may be expressed as [17]:

$$D = \frac{1}{2}\rho C_D A V_r^2 + \frac{\pi}{4}\rho C_M A b \dot{V}_r \qquad (3.1)$$

where: V_r = relative wind velocity $\dot{V}_r$ = relative rate of change of wind velocity, ρ = air density, A = windward area of the structure, b = lateral dimension of the structure, C_D and C_M are constants

This equation is obtained from aerodynamic theory. The ASME standards [2] have taken the above equation and applied appropriate values for C_D and C_M, which results in a much more useful tool for stack analysis. A table of velocity pressure exposure coefficients, based upon the type of terrain and height above ground level is supplied in the standards. The static calculations within STACK1 are, hence, carried out via the standards method described in chapter 5. Given the load per unit length of stack, the deflection in the along wind direction due to the static drag load is readily calculated by

transfer matrices. The detailed calculations are provided in appendix 1, and are included in the newest version of the STACK1 software.

3.4 Dynamic Response and Harmonic Excitation

The vibrations of a stack are a concern of the designer if any of the number of dynamic loads are applied at or near resonance conditions. The first and second bending modes are generally all that are of interest [18], since very little energy is imparted at higher frequencies, as will be shown. Because steel stacks are generally very long, slender structures with relatively high flexibility and low structural damping, the frequency of the first bending mode is usually extremely low, often less than 1 Hz. Various harmonic excitation occurs at very low frequencies as well, so the first mode is generally produces the largest deflections and stresses, although in certain instances the second mode must be investigated as well.

Dynamic wind forces arise from various sources [10]:

- turbulent forces in the earth's boundary layer,
- forces due to local turbulence within the stack's wake, particularly due to vortex shedding, and
- forces induced by motion of the structure.

3.4.1 Atmospheric Turbulence

Atmospheric turbulence can impart significant energy through out a frequency range of about 0.01 Hz to 2 Hz [10]. Figure 3-2 shows a wind-speed spectrum having two

distinct “humps” in the frequency domain. One area essentially represents static loads, and a second region which represents dynamic loads that can cause vibration of the structure.

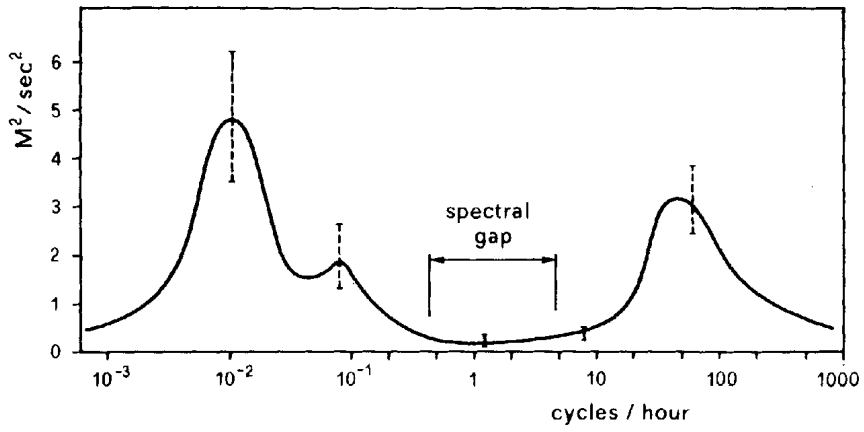

Figure 3-2. Horizontal Wind-Speed Spectrum at Brookhaven National Laboratory at about 100 m (328 ft) height, after Lin [19]

It should be noted that the higher frequency turbulence generally acts along the wind direction, manifesting itself as wind gusts. However, due to the random nature of turbulence, and due to the flow differences across the stack, cross-wind loading can also be imparted. The magnitude of loading due to pure atmospheric turbulence is not typically calculated, rather, the effect of combining the turbulence with the lift forces resulting from vortex shedding is used [20].

3.4.2 Vortex Shedding

Stacks constitute what is known as a bluff structure. A bluff structure is one in which the flow separates from large sections of the structure's surface [21]. The area of turbulent recirculation on the down-wind side of a bluff body is referred to as the *wake*. Under most flow conditions, the wake of a long, slender structure will be unsteady and will shed vortices. The nature of vortex shedding is a well studied phenomenon over a wide range of flow conditions. A typical pattern of vortex shedding in the wake of a cylinder is shown in Figure 3-3. This is the flow profile over a constant diameter cylinder with a constant velocity flow profile.

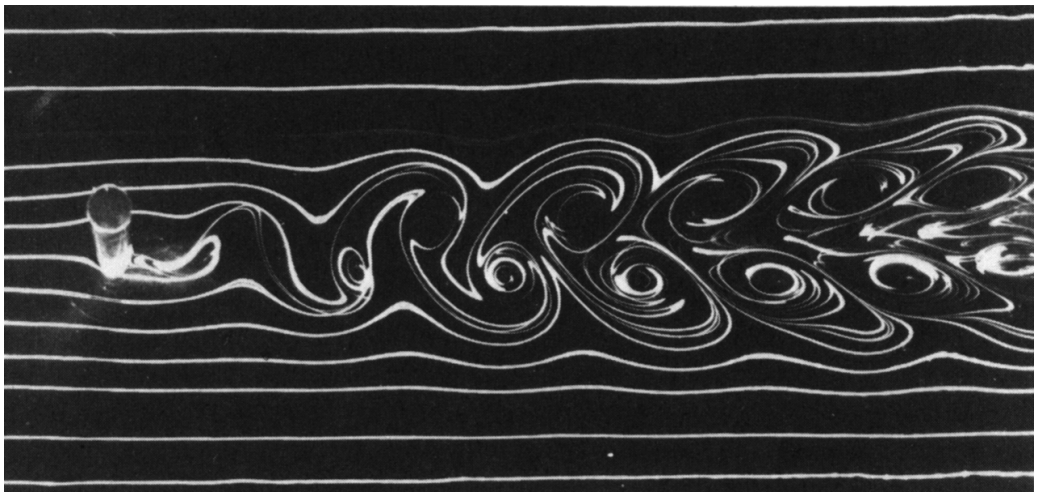

Figure 3-3. Vortex shedding around a cylinder, after Blevins [22]

Vortex shedding around a cylinder has been studied extensively. Vortex shedding from a smooth, circular cylinder at subsonic flows is a function of Reynolds number. The Reynolds number is defined as:

$$Re = \frac{UD}{\nu} \qquad (3.2)$$

where: U = free stream velocity, D = circular diameter, ν = kinematic viscosity (for air, 6.082 ft^2/hr @ 68° F ($15.7x10^{-6}$ m^2/s @ 20° C) [23])

Experimental results have been tabulated for vortex shedding regimes around a smooth circular cylinder of various Reynolds numbers as shown in Figure 3-4.

At very low Reynolds numbers (below $Re = 5$), the fluid follows a smooth, laminar profile around the cylinder. In the range $5 < Re < 45$, separation begins on the back of the cylinder and a symmetric pair of vortices is formed close to the cylinder. The length of the vortices in the along flow direction increases linearly with Reynolds number, reaching a length of three cylinder diameters at $Re = 45$. Beyond this point, the wake becomes unstable and one of the vortices breaks away. A laminar periodic wake of staggered vortices with opposite rotation direction (vortex street) is formed. Between $Re = 150$ and 300, the vortices become turbulent, although the cylinder boundary layer remains laminar. The *subcritical* range is defined as the range of $300 < Re < 1.5x10^5$. In this range, the

laminar boundary layers separate from the cylinder and the vortex shedding is strong and periodic. The vortex street transitions to turbulent in the range $1.5x10^5 < Re < 3.5x10^6$, which is know as the *transitional* range. Lastly, the *supercritical* range, $Re > 3.5x10^6$, periodic vortex shedding is re-established with a turbulent cylinder boundary layer.

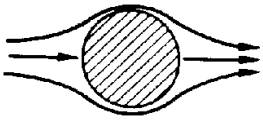

(1) $Re < 5$
REGIME OF UNSEPARETED FLOW

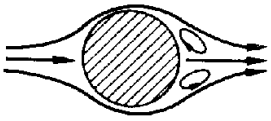

(2) 5 TO 15 < Re < 40
A FIXED PAIR OF F_PPL VORTICES IN WAKE

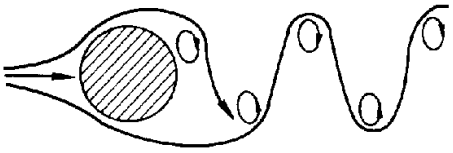

(3) 40 < Re < 90 AND 90 < Re < 150
TWO REGIMES IN WHICH VORTEX STREET IS LAMINAR

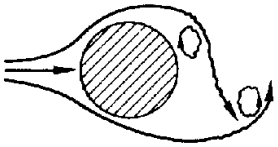

(4) 150 < Re < 300
TRANSITION RANGE TO TURBULENCE IN VORTEX

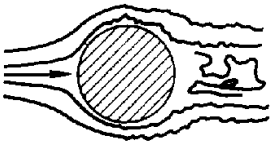

(5) $3x10^5 < Re < 3.5x10^6$
LAMINAR BOUNDARY LAYER HAS UNDERGONE TURBULENT TRANSITION AND WAKE IS NARROWER AND DISORGANIZED

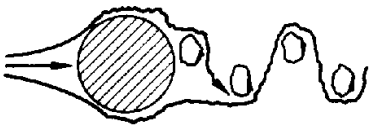

(6) $5.6x10^6 < Re$
RE-ESTABLISHMENT OF TURBULENT VORTEX STREET

Figure 3-4. Vortex shedding regimes around a smooth cylinder, after Blevins [3]

Reynolds numbers associated with large stacks can exceed 10^7, so all of the above flow regimes are possibilities. Wind speeds of above 20 mph (9 m/s) for stacks of cross sectional diameter of 3 ft (0.9 m) or more will produce a turbulent vortex street similar to item (3) and item (4) in Figure 3-4. Vortex shedding causes harmonic loading on a cylinder in both the along wind and cross wind directions. These dynamic loads will cause stack vibration under certain conditions. If a resonance frequency of the stack lies with in the spectrum of vortex shedding frequencies, large across-wind vibration amplitudes could arise if there is not sufficient damping.

A sequence of pressure fields on a cylinder as a vortex is shed is shown in Figure 3-5.

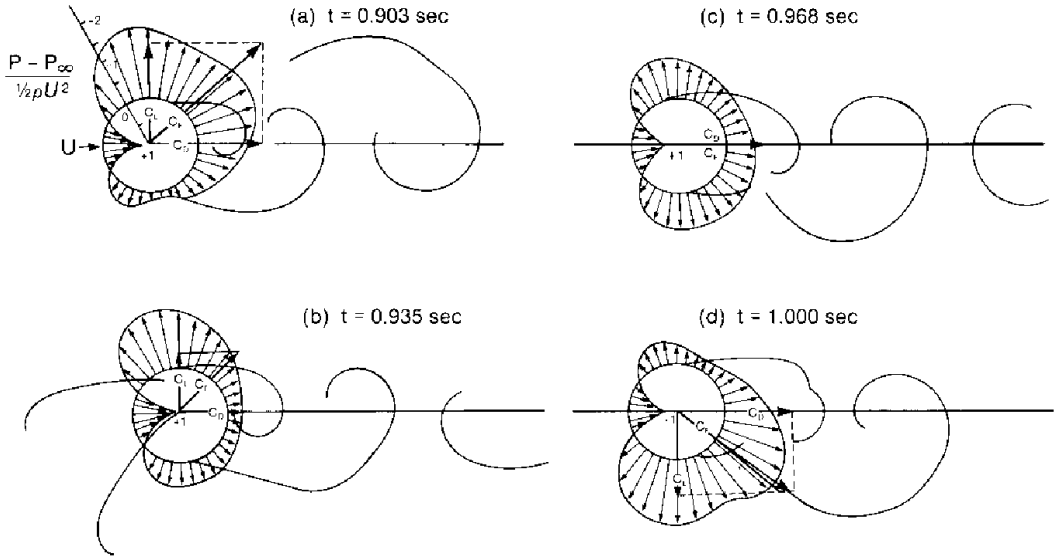

Figure 3-5. A sequence of simultaneous surface pressure fields and wake forms at *Re* = 112,000 for approximately one-third of one cycle of vortex shedding,

after Blevins [24]

In this diagram, it can be seen how the lift force, C_L acts in a direction perpendicular to the flow field, and the drag force, C_D, acts in the along-wind direction.

The magnitude of lift force is given by [25]:

$$F_o(z) = \tfrac{1}{2} C_L \rho u^2(z_{ei}) D(z) \qquad (3.3)$$

where: C_L = lift coefficient; 0.45 for $Re < 2\text{x}10^5$; 0.14 for $2\text{x}10^5 < Re < 2\text{x}10^6$;

0.2 for $2\text{x}10^6 < Re$, ρ = density of air; 1.164 kg/m^3 @ 68° F,

$u(z_{ei})$ = wind speed at height z_{ei}; where z_{ei}=(5/6)*height of stack, and

$D(z)$ = stack diameter at height z

The variation of stack diameter and wind velocity make this lift force vary along the length of the stack. In order to apply the lift forces in the STACK1 code, relationships suggested by the ASME standards [26] should be used to apply the across-wind lift forces. The standards exploit the near-uniform velocity profile on the upper one-third of the stack to provide a lateral force ("lift" force) per unit length that is independent of height. Moreover, the dynamic loads near the top of the stack are much more effective in exciting the first and second modes of concern in this work.

The effect of atmospheric turbulence on the lift force due to the vortex street is much more complicated. Assumptions must be made regarding the nature of the turbulent interaction, and a modified lift force equation can be obtained [20]

$$F_o(z,t) = \_\, C_L \rho u^2(z_{ei}) D(z) \cos(\omega_s t + \psi(t)) \qquad (3.4)$$

where $\psi(t)$ is a slowly varying random process, and ω_s is the frequency of vortex shedding

Since stacks are generally tall and rise above the greatest turbulent effects, the effect of turbulence on the frequency of vortex shedding is, therefore, assumed to be small in this analysis, as it is in the stack design standards [27].

3.4.3 Motion-Induced Forces

Motion-induced forces include those forces in-phase with displacement or acceleration (aerodynamic stiffness or mass) and those forces in phase with velocity (negative aerodynamic damping) or the forces 180° out-of-phase (positive aerodynamic damping) [10]. The effects of negative aerodynamic damping can be quite substantial in the *cross wind direction only* in the range just above $U^* > 1/S$, where

$$U^{*}=U/f_{o}B \qquad (3.5)$$

where: U = mean wind speed, f_o = frequency of vibration, B = breadth of structure, S = Strouhal number

Negative aerodynamic damping can cause excessive vibration amplitudes. Experiments have shown that negative aerodynamic damping can exist on the same magnitude as structural damping when regular vortex shedding is present [28]. If the frequency of vortex shedding occurs at a structural resonance, the effects of negative aerodynamic damping can cause extremely large tip oscillations. Under 'ideal' conditions unbounded vibration amplitudes could occur, resulting in catastrophic failure. This is therefore an extremely important consideration in stack design. The natural frequencies should be designed into the structure at spectral points where periodic vortex shedding will not occur.

3.5 Across-Wind Response

The aforementioned variables must be considered when calculating across-wind responses. Along-wind responses requires only a knowledge of the drag coefficient [10]. The along-wind response is then predicted by a "gust-factor", which is outlined in the ASME Stack Standards [27] and ASCE standards [6] and is presented in detail in appendix I.

In calculating the across-wind response due to vortex shedding, the main concern is whether or not near-resonant conditions can occur. The frequency of vortex shedding is given by the simple formula [29]

$$f_s = SU/D \text{ Hz} \qquad (3.6)$$

where: S = Strouhal number, typically used as 0.2 for single stacks, but can vary due to Reynolds number and multiple stacks [27], U = free stream flow velocity, D = stack diameter U and D must have consistent units.

The critical speed, V_c, is the speed at which wake-induced excitation reaches a maximum. For long slender structures, V_c typically occurs below the design speed, V_D, which is the maximum wind speed the stack is designed to withstand [27].

$$V_c = f_1 d/S \qquad (3.7)$$

where f_1 = the frequency of the first harmonic,

d = the mean diameter of the upper 1/3 of stack, ft.

To accurately predict the magnitude of across wind forces for a given stack design, the range of wind speeds for a given geographical area must be know.

From the contour map in Figure 3-7, the maximum expected wind velocity for a given geographical region can be obtained. This wind velocity is called the "basic design speed" (V_R), because it is the maximum speed expected to occur at a height of thirty-three feet above the ground with a return period of ten years [27]. It is under this wind condition that the maximum static and dynamic loading will occur. A given value for V_R can be used in eqn. 3.4 to find the magnitude of the harmonic loading. Equation 3.4 provides the necessary assumptions to obtain a uniform harmonic load on the stack.

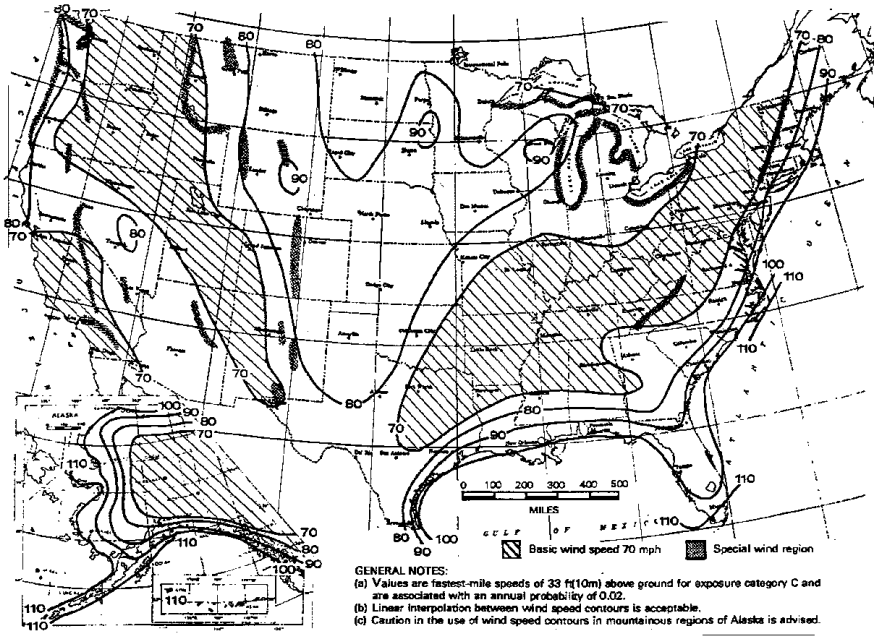

Figure 3-7. Wind design speed contours within the United States, after ASME standards [14]

The ASME Standards [2] provide a set of comprehensive wind response calculations that incorporates the harmonic response of the stack. This method of finding the stack response is currently coded in STACK1. Based on these calculations, STACK1 advises the user of the expected vibration amplitudes.

Chapter 4: Transfer Matrix Method

4.1 Introduction

The transfer matrix method is a method for finding the static and dynamic properties of an elastic system. The basic principle behind this method is that of breaking up a complicated system into individual parts with simple elastic and dynamic properties that can be expressed in matrix form [29]. When these individual matrices are arranged in a prescribed fashion and multiplied together, the static and dynamic behavior of the entire system is readily calculated. Many structures encountered in practice consist of a number of elements linked together end to end in a chain-like configuration. Examples of this type of system include continuous beams, turbine rotors, crankshafts, pressure vessels, etc. The transfer matrix method provides a quick and efficient analysis of such systems simply by multiplying successive elemental transfer matrices together. Therefore, this method is ideal for analyzing stacks with wind loading, which will be treated as uniform continuous beams with external distributed loading.

4.2 Coordinate System and Sign Convention

The first step in developing transfer matrix theory is to establish a coordinate system. A right-handed Cartesian coordinate system is used with the x-axis coinciding with the centroidal axis of the beam. Looking at a small beam section, two faces will be exposed. The face whose outward normal points in the positive x-direction is a positive face. The

face whose outward normal points in the negative direction is a negative face, as shown in Figure 4-1. Positive displacements refer to the positive directions of the coordinate system. Force pairs are considered positive if the force acts on a positive face and is directed in the positive direction, or if the force acts on a negative face and acts in the negative direction.

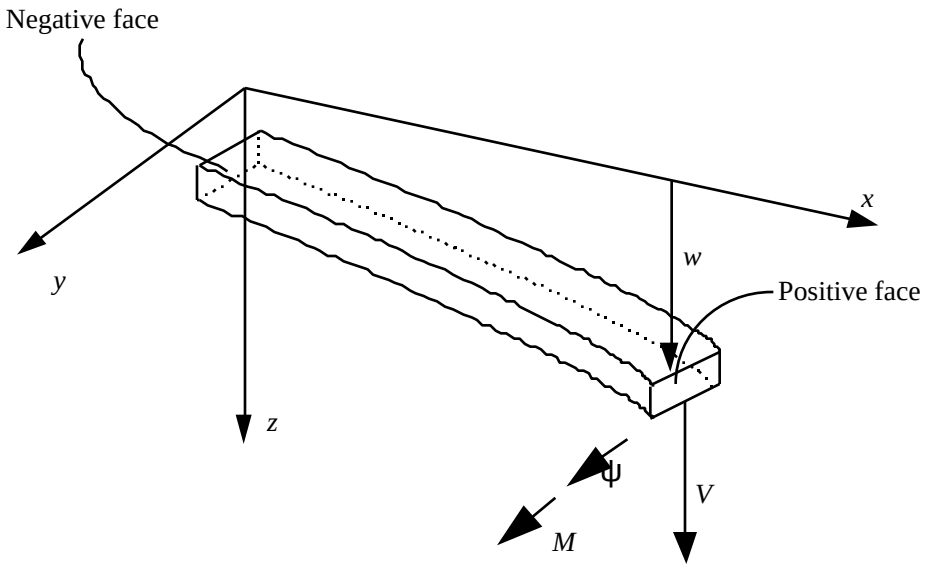

Figure 4-1. Transfer matrix coordinate system

4.3 State Vector and Transfer Matrix

A state vector is a column vector that contains all the displacements and internal forces of a structure at a given point. For example, in the case of a simple spring, the state vector would consist of the displacement of the spring, x_i, and the associated internal force, N_i. In matrix notation this state vector, z, would be written with the displacements on the top, and internal forces on the bottom:

$$z_i = \begin{Bmatrix} x_i \\ N_i \end{Bmatrix} = \begin{Bmatrix} x \\ N_i \end{Bmatrix}_i \tag{4.1}$$

A more complicated state vector exists for a straight beam. The displacements at point i are the deflection w_i, and the slope ψ_i. The internal forces are the shear force, V_i, and the moment, M_i.

$$z_i = \begin{Bmatrix} w \\ \psi \\ V \\ M \end{Bmatrix}_i \tag{4.2}$$

The placement of these components are such that a force and the corresponding complementary displacement (w and V, ψ and M) are in positions that are mirrored about the center of the column vector.

4.4 Transfer Matrix Procedure

In order to analyze complex structures with the transfer matrix method, the structure first needs to be divided into simple sections. For each of these simple sections, a matrix is used to describe how the displacements and forces interact with each other. For example, consider the following spring-mass system that is vibrating with circular frequency ω in Figure 4-2.

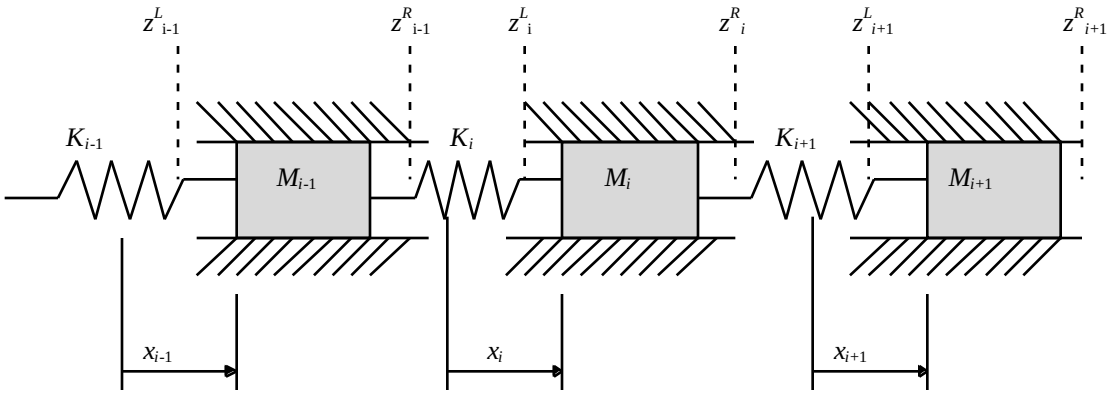

Figure 4-2. Spring - mass system, adapted from Pestel and Leckie [28]

The mass M_{i-1} is attached to mass M_i by a massless spring of stiffness k_i. The state vector immediately to the left of mass m_i is labeled as z_i^L. The state vector immediately to the right of mass m_{i-1} is labeled as $z_{i-1}{}^R$. The internal forces of spring k_{i-1} are shown in Figure 4-3.

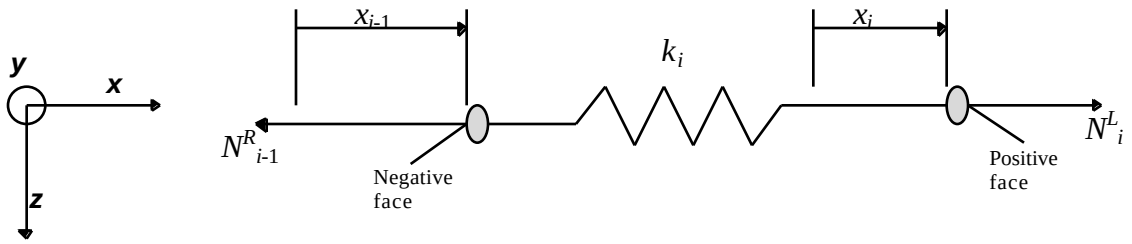

Figure 4-3. Free-body diagram of spring

Because the spring is massless, the forces acting on either end of the spring are equivalent.

$$N_{i-1}{}^R = N_i^L \tag{4.3}$$

From the stiffness definition for a linear spring, the internal force acting through the spring is:

$$N_{i-1}{}^R = N_i^L = k_i(x_i - x_{i-1}) \tag{4.4}$$

Rewriting these equations yields

$$x_i = x_{i-1} + N_{i-1}{}^R / k_i \tag{4.5}$$

$$N_i^L = (0)\, x_{i-1} + N_{i-1}^R \tag{4.6}$$

In matrix form,

$$\begin{Bmatrix} x \\ N \end{Bmatrix}_i^L = \begin{bmatrix} 1 & 1/k_i \\ 0 & 1 \end{bmatrix} * \begin{Bmatrix} x \\ N \end{Bmatrix}_{i-1}^R \tag{4.7}$$

or

$$\{z\}_i^L = [F_i]\{z\}_{i-1}^R \tag{4.8}$$

This equation provides a relation between the two state vectors on either side of the spring. The matrix $[F_i]$ is know as the *field transfer matrix*.

In a similar manner, the transfer matrix between two state vectors on either side of the mass can be derived. From the free-body diagram in Figure 4-4, it can be seen that the displacements on either side of the infinitely rigid, point mass will be equal.

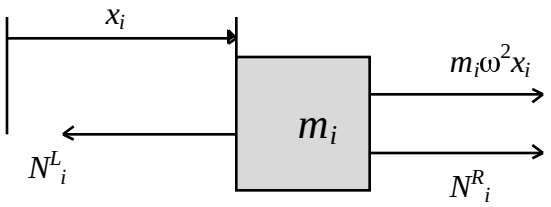

Figure 4-4. Free-body diagram of a mass

$$x_i^R = x_i^L \tag{4.9}$$

Summing the forces and rearranging from the free body diagram,

$$N_i^R = N_i^L - m_i\omega^2 x_i \tag{4.10}$$

In matrix form, these two equations can be represented as follows

$$\begin{Bmatrix} x \\ N \end{Bmatrix}_i^R = \begin{bmatrix} 1 & 0 \\ -m_i\omega^2 & 1 \end{bmatrix} * \begin{Bmatrix} x \\ N \end{Bmatrix}_i^L \tag{4.11}$$

or

$$\{z\}_i^R = [P]_i\{z\}_i^L \tag{4.12}$$

Where $[P_i]$ is referred to as the *point transfer matrix*.

From these two transfer matrices, a variety of spring - mass problems can easily be analyzed. As mentioned before, $[P_i]$ is the point transfer matrix for mass m_i, and $[F_i]$ is the field transfer matrix for spring k_i. To find the relation between the state vectors on either side of the series of the structure shown in Figure 4.2, the internal transfer matrices are multiplied together in the following fashion.

$$z_{i-1}^{R} = P_{i-1} z_{i-1}^{L}$$

$$z_i^{L} = F_i z_{i-1}^{R} = F_i P_{i-1} z_{i-1}^{L}$$

$$z_i^{R} = P_i z_i^{L} = P_i F_i P_{i-1} z_{i-1}^{L}$$

$$z_{i+1}^{L} = F_{i+1} z_i^{R} = F_{i+1} P_i F_i P_{i-1} z_{i-1}^{L}$$

$$z_{i+1}^{R} = P_{i+1} z_{i+1}^{L} = P_{i+1} F_{i+1} P_i F_i P_{i-1} z_{i-1}^{L} \qquad (4.13)$$

The above transfer matrix multiplication can written as:

$$z_{i+1}^{R} = U z_{i-1}^{L} \qquad (4.14)$$

Where U is the global transfer matrix.

4.5 Transfer Matrices for Planar Vibrations of a Straight Beam

In order to analyze stacks, transfer matrices for beam sections must be used.

The above procedure can be extended to the analysis of beam vibrations. In order to extract the eigenvalues for a continuum beam, the beam will first be modeled by replacing

the actual beam with a lumped-mass model which has the same bending stiffness. This type of lumped-mass beam is easily analyzed by transfer matrices. The sign convention established earlier will be applied to the beam model. As noted before, the two displacements are the deflection, *w*, and the slope, ψ, and the internal forces are the shear force, *V*, and the bending moment, *M*. A single, massless beam segment is shown in Figure 4-5 with the appropriate end forces and displacements .

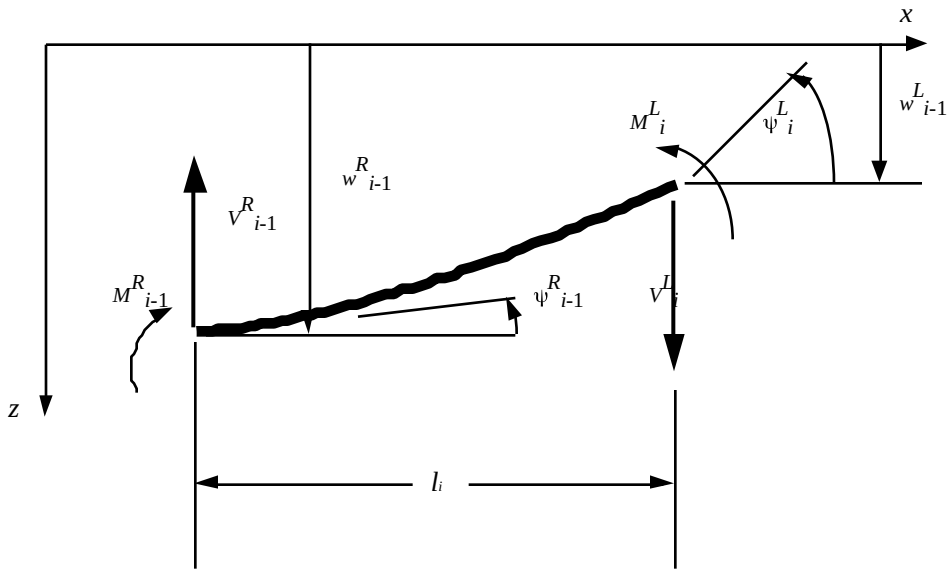

Figure 4-5. End forces and deflections for a massless beam

Because the beam is massless, the sum of the vertical forces must equal zero, and the sum of the moments about any point must equal zero. These two equations are:

$$V_i^L - V_{i-1}^R = 0 \tag{4.15a}$$

$$V_i^L = V_{i-1}^R \tag{4.15b}$$

$$M_i^L - M_{i-1}^R - V_i^L l_i = 0 \tag{4.16a}$$

$$M_i^L = M_{i-1}^R + V_i^L l_i \tag{4.16b}$$

Recalling two further equations for the end deflection and slope of a cantilever beam with flexural stiffness EJ subjected to moment M and shear V at its free end from elemental beam theory [33]:

$$w = -\frac{Ml^2}{2EJ} + \frac{Vl^3}{3EJ} \tag{4.17}$$

$$\psi = \frac{Ml}{EJ} - \frac{Vl^2}{2EJ} \tag{4.18}$$

Applying these equations to Figure 4-5,

$$w_i^L = w_{i-1}^R - \psi_{i-1}^R l_i - M_i^L \frac{l_i^2}{2(EJ)_i} + V_i^L \frac{l_i^3}{3(EJ)_i} \tag{4.19}$$

and

$$\psi_i^L = \psi_{i-1}^R + M_i^L \frac{l_i}{(EJ)_i} - V_i^L \frac{l_i^2}{2(EJ)_i} \tag{4.20}$$

In order to express eqns. (4.15b), (4.16b), (4.19), and (4.20) in state vector form, they are arranged in columns as follows:

$$w_i^L = w_{i-1}^R - \psi_{i-1}^R l_i - M_i^L \frac{l_i^2}{2(EJ)_i} + V_i^L \frac{l_i^3}{3(EJ)_i} \tag{4.21a}$$

$$y_i^L = (0)w + \psi_{i-1}^R + M_i^L \frac{l_i}{(EJ)_i} - V_i^L \frac{l_i^2}{2(EJ)_i} \tag{4.21b}$$

$$V_i^L = (0)w + (0)\psi + (0)M + V_{i-1}^R \tag{4.21c}$$

$$M_i^L = (0)w + (0)\psi + M_{i-1}^R + V_i^L l_i \tag{4.21d}$$

or, in matrix notation,

$$\begin{Bmatrix} -w \\ \psi \\ M \\ V \end{Bmatrix}_i^L = \begin{bmatrix} 1 & l & \frac{l^2}{2EJ} & \frac{l^3}{6EJ} \\ 0 & 1 & \frac{l}{EJ} & \frac{l^2}{2EJ} \\ 0 & 0 & 1 & l \\ 0 & 0 & 0 & 1 \end{bmatrix}_i * \begin{Bmatrix} -w \\ \psi \\ M \\ V \end{Bmatrix}_{i-1}^R \qquad (4.22)$$

$$\text{or} \qquad \{z\}_i^L = [F]_i \{z\}_{i-1}^L$$

where the matrix $[F_i]$ is the field matrix for the massless beam.

In order to develop a transfer matrix for the lumped mass, relations are needed between the left and right sides of the mass. It is noted that since the lumped mass is of zero length, the deflection, slope, and moment are the same on either side of the mass.

$$w_i^R = w_i^L \qquad \psi_i^R = \psi_i^L \qquad M_i^R = M_i^L \qquad (4.23a)$$

The shear term, however is not the same across a vibrating mass. The inertia of the mass introduces a discontinuity in shear. From the free body diagram of the mass, Figure 4-6, equilibrium yields:

$$V_i^R = V_i^L - m_i \omega^2 w_i \qquad (4.23b)$$

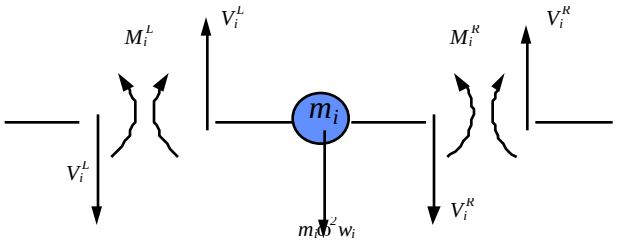

Figure 4-6. Free-body diagram of mass m_i, after Pestel and Leckie, [33]

In matrix form, the above four equations become:

$$\begin{bmatrix} -w \\ M \\ V \end{bmatrix}_i^R = \begin{bmatrix} 1 & 0 & 0 & 0 \\ 0 & 1 & 0 & 0 \\ 0 & 0 & 1 & 0 \\ m\omega^2 & 0 & 0 & 1 \end{bmatrix}_i * \begin{bmatrix} -w \\ M \\ V \end{bmatrix}_i^L \tag{4.24}$$

or

$$\{z\}_i^R = [P]_i \{z\}_i^L$$

where the matrix $[P]_i$ is the point matrix for a vibrating mass.

Given the field matrix $[F]_i$ and the point matrix $[P]_i$ for a lumped-mass beam, the natural frequencies can easily be calculated. Consider a simple cantilever with a concentrated end mass and flexural stiffness EJ as shown in Figure 4-7.

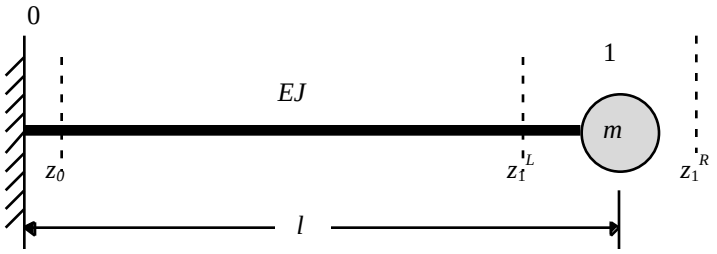

Figure 4-7. Cantilever with concentrated end mass, after Pestel and Leckie [34]

Using the previously developed transfer matrices:

$$z_1^R = \begin{bmatrix} 1 & 0 & 0 & 0 \\ 0 & 1 & 0 & 0 \\ 0 & 0 & 1 & 0 \\ -m\omega^2 & 0 & 0 & 1 \end{bmatrix} * z_1^L \tag{4.25}$$

$$z_1^L = \begin{bmatrix} 1 & l & \frac{l^2}{2EJ} & \frac{l^3}{6EJ} \\ 0 & 1 & \frac{l}{EJ} & \frac{l^2}{2EJ} \\ 0 & 0 & 1 & l \\ 0 & 0 & 0 & 1 \end{bmatrix} * z_0^R \tag{4.26}$$

from which we obtain the relationship between $\{z\}_1^R$ and $\{z\}_0^R$:

$$\{z\}_1^R = [P]_1[F]_1\{z\}_0^R$$

or

$$\begin{Bmatrix} -w \\ \psi \\ M \\ V \end{Bmatrix}_1 = \begin{bmatrix} 1 & l & \frac{l^2}{2EJ} & \frac{l^3}{6EJ} \\ 0 & 1 & \frac{l}{EJ} & \frac{l^2}{2EJ} \\ 0 & 0 & 1 & l \\ m\omega^2 & m\omega^2 l & \frac{m\omega^2 l^2}{2EJ} & 1+\frac{m\omega^2 l^3}{6EJ} \end{bmatrix} * \begin{Bmatrix} -w \\ \psi \\ M \\ V \end{Bmatrix}_0 \quad (4.27)$$

For this example, $M_1^R = V_1^R = w_0 = \psi_0 = 0$, which leads to the following:

$$-w_1^R = l^2/(2EJ) * M_0^R + l^3/(6EJ) * V_0^R \quad (4.28a)$$

$$\psi_1^R = l/(EJ) * M_0^R + l^2/(2EJ) * V_0^R \quad (4.28b)$$

$$0 = M_0^R + l * V_0^R \quad (4.28c)$$

$$0 = m\omega^2 l^2/(2EJ) * M_0^R + (1 + m\omega^2 l^2/(6EJ))V_0^R \quad (4.28d)$$

Rewriting the last two equations in matrix form,

$$\begin{bmatrix} 1 & l \\ \frac{m\omega^2 l^2}{2EJ} & 1+\frac{m\omega^2 l^3}{6EJ} \end{bmatrix} \begin{Bmatrix} M \\ V \end{Bmatrix}_o^R = \begin{Bmatrix} 0 \\ 0 \end{Bmatrix} \quad (4.29)$$

For the last two equations to be satisfied, the non-trivial solution demands that the determinant of the coefficient matrix be zero [35]:

$$\begin{vmatrix} 1 & l \\ \frac{m\omega^2 l^2}{2EJ} & 1+\frac{m\omega^2 l^3}{6EJ} \end{vmatrix} = 0 \quad (4.30)$$

By expanding the determinant, the natural frequency is found to be:

$$\omega^2 = \frac{3EJ}{ml^3}$$

or

$$\omega = \sqrt{\frac{3EJ}{ml^3}} \tag{4.31}$$

4.6 Complex Beams, Elimination of Intermediate State Vectors

The application of transfer matrices to more complex beams will now be discussed. Consider a complex beam with multiple lumped masses and discrete massless beam sections as shown in Figure 4-8.

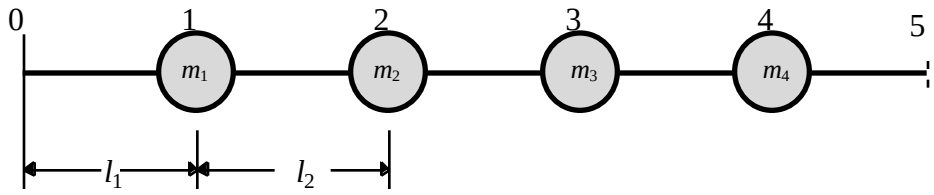

Figure 4-8. Beam with discrete masses, after Pestel and Leckie [36]

Since the transfer matrices for the individual components of this beam are known, the transfer matrix for the entire beam is easily found. Recalling the matrices $[F]_i$ and $[P]_i$ for a beam section, the following relations exist between adjacent state vectors, as in the spring mass system discussed earlier.

$$z_1^L = F_1 z_0^R \quad z_1^R = P_1 z_1^L \quad z_2^L = F_2 z_1^R \quad \ldots \quad z_6^L = F_6 z_5^R \quad z_6^R = P_6 z_6^L \quad z_7^L = F_7 z_6^R$$

$$z_7 = F_7 P_6 \, F_6 P_5 \, F_5 P_4 F_4 P_3 \, F_3 P_2 F_2 P_1 F_1 z_0$$

$$z_7 = U z_0 \tag{4.32}$$

Because the elements u_{ik} of the global transfer matrix $[U]$ are know functions of the natural frequency ω, this determinant serves as the characteristic equation for computing the natural frequencies. Because there are four discrete masses in this system, the expansion of the determinant will lead to an equation of fourth order in ω^2.

In modeling stacks, only one type of boundary condition is considered, that of fixed base with a free end. If the flexibility and damping of the stack foundation is of concern, this can be modeled using a translational and rotational spring in an additional section underneath the stack. The left side of the model will have a fixed boundary condition regardless. Because of the prescribed boundary conditions, it is not necessary to carry out the complete matrix multiplication. For example, consider the three section beam in Figure 4-9 where the transfer matrices for section A, B, and C are known. The full matrix multiplication would be set up as follows:

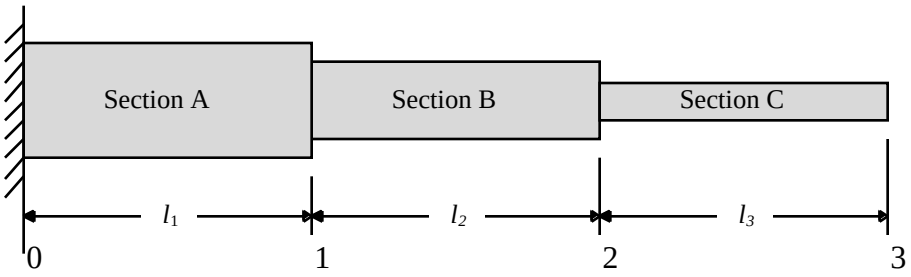

Figure 4-9. Fixed - free three section beam

Boundary conditions for fixed - free beam:

$$M_1 = V_1 = 0$$

$$w_0 = \psi_0 = 0$$

For this beam:

$$z_1 = Az_0 \qquad z_2 = BAz_0 \qquad z_3 = CBAz_0$$

When matrix multiplication is carried out, as shown below, the first and second columns are multiplied by zero and thus play no part in the calculation. Therefore, elements of matrices A, D, and E that are in the first and second columns can be omitted from the multiplication.

$$A\begin{bmatrix} a_{11} & a_{12} & a_{13} & a_{14} \\ a_{21} & a_{22} & a_{23} & a_{24} \\ a_{31} & a_{32} & a_{33} & a_{34} \\ a_{41} & a_{42} & a_{43} & a_{44} \end{bmatrix} * \begin{Bmatrix} 0 \\ 0 \\ M \\ V \end{Bmatrix}_0 = z_1 \quad (4.33a)$$

$$B\begin{bmatrix} b_{11} & b_{12} & b_{13} & b_{14} \\ b_{21} & b_{22} & b_{23} & b_{24} \\ b_{31} & b_{32} & b_{33} & b_{34} \\ b_{41} & b_{42} & b_{43} & b_{44} \end{bmatrix} * \begin{bmatrix} d_{11} & d_{12} & d_{13} & d_{14} \\ d_{21} & d_{22} & d_{23} & d_{24} \\ d_{31} & d_{32} & d_{33} & d_{34} \\ d_{41} & d_{42} & d_{43} & d_{44} \end{bmatrix} * \begin{Bmatrix} 0 \\ 0 \\ M \\ V \end{Bmatrix}_0 = z_2$$

$$C\begin{bmatrix} c_{11} & c_{12} & c_{13} & c_{14} \\ c_{21} & c_{22} & c_{23} & c_{24} \\ c_{31} & c_{32} & c_{33} & c_{34} \\ c_{41} & c_{42} & c_{43} & c_{44} \end{bmatrix} * \begin{bmatrix} e_{11} & e_{12} & e_{13} & e_{14} \\ e_{21} & e_{22} & e_{23} & e_{24} \\ e_{31} & e_{32} & e_{33} & e_{34} \\ e_{41} & e_{42} & e_{43} & e_{44} \end{bmatrix} * \begin{Bmatrix} 0 \\ 0 \\ M \\ V \end{Bmatrix}_0 = z_3 \qquad (4.33b)$$

(4.33c)

The abridged version is thus:

$$A\begin{bmatrix} a_{13} & a_{14} \\ a_{23} & a_{24} \\ a_{33} & a_{34} \\ a_{43} & a_{44} \end{bmatrix} * \begin{Bmatrix} M \\ V \end{Bmatrix}_0 = z_1 \qquad (4.34a)$$

$$B\begin{bmatrix} b_{11} & b_{12} & b_{13} & b_{14} \\ b_{21} & b_{22} & b_{23} & b_{24} \\ b_{31} & b_{32} & b_{33} & b_{34} \\ b_{41} & b_{42} & b_{43} & b_{44} \end{bmatrix} * \begin{bmatrix} d_{13} & d_{14} \\ d_{23} & d_{24} \\ d_{33} & d_{34} \\ d_{43} & d_{44} \end{bmatrix} * \begin{Bmatrix} M \\ V \end{Bmatrix}_0 = z_2$$

$$C\begin{bmatrix} c_{11} & c_{12} & c_{13} & c_{14} \\ c_{21} & c_{22} & c_{23} & c_{24} \\ c_{31} & c_{32} & c_{33} & c_{34} \\ c_{41} & c_{42} & c_{43} & c_{44} \end{bmatrix} * \begin{bmatrix} e_{13} & e_{14} \\ e_{23} & e_{24} \\ e_{33} & e_{34} \\ e_{43} & e_{44} \end{bmatrix} * \begin{Bmatrix} M \\ V \end{Bmatrix}_0 = z_3 = \begin{Bmatrix} -w \\ \psi \end{Bmatrix}_3 \qquad (4.34b)$$

(4.34c)

The above multiplication scheme yields less multiplication than takes place in eqns. (4.33) and is, therefore, more computationally efficient.

4.7 Steady-state forced vibrations and statics

In the previous sections it has been shown how transfer matrices can be used to find the natural frequencies of an elastic system. Once the natural frequencies are known, it is possible to solve general cases of forced undamped vibrations. Recalling from basic vibrations that if a system is forced at a circular frequency, Ω, the system will vibrate in steady state with the same circular frequency [37]. Because of this fact, transfer matrices can be extended to the problem of steady-state forced vibrations and statics (Ω = 0). Now, the corresponding relations when a length of beam is subjected to a uniformly distributed harmonic load $q(t) = Q\cos(\Omega t)$ is studied as shown in Figure 4-10.

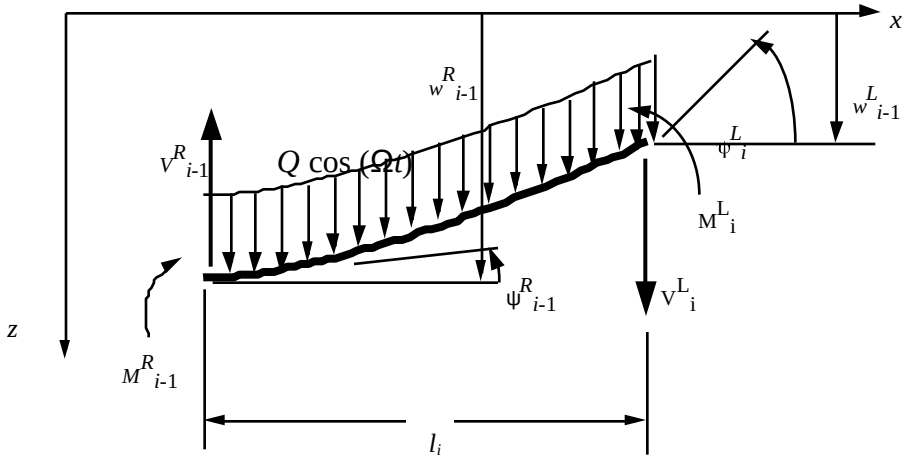

Figure 4-10. Beam section with uniformly distributed load $q(t) = Q\cos(\Omega t)$, after Pestel and Leckie [38]

From equilibrium conditions we have for a massless beam [38]:

$$V_i^L = V_{i-1}{}^R - q_i l_i \qquad M_i^L = M_{i-1}{}^R + V_i^L\, l_i - q_i l_i^2 / 2 \tag{4.35}$$

Also, from strength of materials, we obtain the following:

$$w_i^L = w_{i-1}^R - \psi_{i-1}^R l_i - M_i^L \frac{l_i^2}{2(EJ)_i} + V_i^L \frac{l_i^3}{3(EJ)_i} + \frac{q_i l_i^2}{8EJ_i} \tag{4.36}$$

$$\psi_i^L = \psi_{i-1}^R + M_i^L \frac{l_i}{(EJ)_i} - V_i^L \frac{l_i^2}{2(EJ)_i} + \frac{q_i l_i^3}{6EJ_i} \tag{4.37}$$

The elimination of M_i^L and V_i^L from the right-hand side of the equations gives:

$$-w_i^L = -w_{i-1}^R + y_{i-1}^R l_i + M_{i-1}^R \frac{l_i^2}{2(EJ)_i} + V_{i-1}^R \frac{l_i^3}{6(EJ)_i} + \frac{q_i l_i^4}{24EJ_i} \tag{4.38}$$

$$\psi_i^L = \psi_{i-1}^R + M_{i-1}^R \frac{l_i}{(EJ)_i} + V_{i-1}^R \frac{l_i^2}{2(EJ)_i} + \frac{q_i l_i^3}{6EJ_i} \tag{4.39}$$

Introducing the identity 1=1 into the lower row of the matrices to facilitate matrix multiplication, the above equations can be written as:

$$\begin{Bmatrix} w \\ \psi \\ M \\ V \\ 1 \end{Bmatrix}_i^L = \begin{bmatrix} 1 & -l & \frac{-l^2}{2EJ} & \frac{-l^3}{6EJ} & \frac{-ql^4}{24EJ} \\ 0 & 1 & \frac{l}{EJ} & \frac{l^2}{2EJ} & \frac{-ql^3}{6EJ} \\ 0 & 0 & 1 & l & \frac{-ql^2}{2} \\ 0 & 0 & 0 & 1 & -ql \\ 0 & 0 & 0 & 0 & 1 \end{bmatrix}_i * \begin{Bmatrix} w \\ \psi \\ M \\ V \\ 1 \end{Bmatrix}_{i-1}^R \qquad (4.40)$$

Or: $\{\boldsymbol{z}\}_i^L = [\boldsymbol{F}]_i \{\boldsymbol{z}\}_{i-1}^R$

where $\{\boldsymbol{z}\}$ is the extended state vector, and $[\boldsymbol{F}]$ is the extended field transfer matrix.

Figure 4-11 shows a massless two section beam subjected harmonic loading $q_1(t)$ and $q_2(t)$:

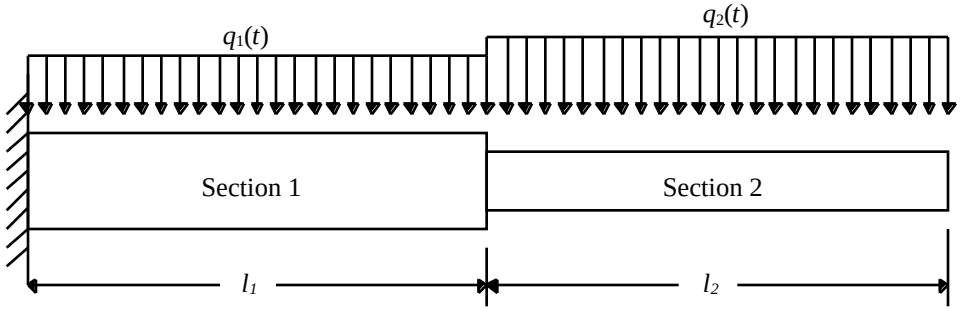

Figure 4-11. Example two section beam with uniform harmonic loading

With the fixed left end of the structure, $w_o = \psi_o = 0$. Therefore the first and second columns of the matrix products can be dropped. At the free end, $M_2 = V_2 = 0$.

$$\{z\}_2 = [F]_2\{z\}_1 \qquad \{z\}_1 = [F]_1\{z\}_0$$

$$\{z\}_2 = [F]_2[F]_1\{z\}_0$$

$$\begin{Bmatrix} -w \\ \psi \\ 1 \end{Bmatrix}_2 = \begin{bmatrix} 1 & -l_2 & \frac{-l_2^2}{2EJ_2} & \frac{-l_2^3}{6EJ_2} & \frac{-q_2 l_2^4}{24EJ_2} \\ 0 & 1 & \frac{l_2}{EJ_2} & \frac{l_2^2}{2EJ_2} & \frac{-q_2 l_2^3}{6EJ_2} \\ 0 & 0 & 1 & l & \frac{-q_2 l_2^2}{2} \\ 0 & 0 & 0 & 1 & -q_2 l_2 \\ 0 & 0 & 0 & 0 & 1 \end{bmatrix} * \begin{bmatrix} \frac{-l_1^2}{2EJ_2} & \frac{-l_1^3}{6EJ_1} & \frac{-q_1 l_1^4}{24EJ_1} \\ \frac{l_1}{EJ_1} & \frac{l_1^2}{2EJ_1} & \frac{-q_1 l_1^3}{6EJ_1} \\ 1 & l & \frac{-q_1 l_1^2}{2} \\ 0 & 1 & -q_1 l_1 \\ 0 & 0 & 1 \end{bmatrix} * \begin{Bmatrix} M \\ V \\ 1 \end{Bmatrix}_0 =$$

$$\begin{bmatrix} (a) & (b) & (c) \\ (d) & (e) & (f) \\ (g) & (h) & (i) \\ (j) & (k) & (l) \\ (m) & (n) & (o) \end{bmatrix} \tag{4.41}$$

With the matrix products as:

$(a) = \dfrac{-l_1^{\,2} - 2l_1 l_2}{2EJ_1} - \dfrac{l_2^{\,2}}{2EJ_2}$

$(b) = \dfrac{-l_1^{\,3} - 3l_1^{\,2} l_2}{6EJ_1} - \dfrac{3l_2^{\,2} l_1 - l_2^{\,3}}{6EJ_2}$

$(c) = \dfrac{-q_1 l_1^{\,4} + 4q_1 l_1^{\,3} l_2}{24EJ_1} + \dfrac{2l_2^{\,3}(q_1 l_1^{\,2}) - q_2 l_2^{\,4}}{24EJ_2}$

$(d) = \dfrac{l_1}{EJ_1} + \dfrac{l_2}{EJ_2}$

$(e) = \dfrac{l_1^{\,2}}{2EJ_1} - \dfrac{2l_1 l_2 + l_2^2}{2EJ_2}$

$(f) = \dfrac{-q_1 l_1^{\,3}}{6EJ_1} - \dfrac{3q_1 l_1^{\,2} l_2 - 3q_1 l_1 l_2^{\,2} - q_2 l_2^{\,3}}{6EJ_2}$

$(g) = 1$

$(h) = l_1 + l_2$

$(i) = -q_1 L_1 L_2 - \dfrac{(q_1 l_1^{\,2} + q_2 l_2^2)}{2}$

$(j) = 0$

$(k) = 1$

$(l) = q_1 L_1 - q_2 L_2$

$(m) = 0$

$(n) = 0$

$(o) = 0$

To find values for w_o, ψ_o, M_2 and V_2, the equations will be simplified by substituting in for the following constants, with the loads q_1 and q_2 as static loads for simplicity:

Section 1	Section 2
D_c = 20 in.	D_c = 14 in.
T_k = 1 in.	T_k = 0.5 in.
L_1 = 100 in.	L_2 = 100 in.
$J_1 = (\pi/64)*(21^4 - 19^4) = 3149.5$ in^4	$J_2 = (\pi/64)*(14.5^4 - 13.5^4) = 539.5$ in^4
E = 3x10^7 psi	E = 3x10^7 psi
q_1 = 8 lb/in	q_2 = 12 lb/in

The following five relations are obtained by carrying out the matrix multiplication and plugging in the above constants.

(1) $-4.67\text{x}10^{-7}\ M_o - 2.063\text{x}10^{-5}\ V_o + .409 = w_2$

(2) $7.23\text{x}10^{-9}\ M_o + 9.788\text{x}10^{-7}\ V_o + 1.09\text{x}10^{-4} = \psi_2$

(3) $M_o + 200\ V_o - 1.8\text{x}10^{5} = 0$

(4) $V_o - 400 = 0$

(5) $1 = 1$

From these equations, the final results can be obtained:

$$V_o = 2000 \text{ psi}$$

$$M_o = -300{,}000 \text{ lb-in}$$

$$\psi_2 = -0.00072 \text{ rad}$$

$$w_2 = 0.180 \text{ in}$$

From the preceding examples, it is apparent how efficiently transfer matrices can be used to analyze static and dynamic systems. The only requirement is that transfer matrices for all of the system's components be known. The above example can easily be extended to a beam with distributed mass simply by using the correct transfer matrices. It is of great practical value to have a catalogue of the most important transfer matrices available, so that when a system is to be analyzed, the individual matrices can be linked together to

form an appropriate solution (various transfer matrices are cataloged in Pestel and Leckie [38]).

This type of analysis is ideal for implementation into a computer program. Various transfer matrices were programmed into the STACK1 code so that the user would have an extremely quick and easy tool to analyze many different types of systems. It is by this program that all of the stack analyses were performed.

Chapter 5: BEAM8 Modifications and Implementation of ASME and ASCE Standards to Generate STACK1

5.1 Introduction

In order to model stack geometry in the STACK1 program, various program changes were made. Some modeling options that are irrelevant to stacks were removed in order to make room for the added features. The user interface was modified to create an environment that is more user friendly for designing stacks. One of the most extensively researched aspects of stack design for this thesis was the behavior of tapered beams. A substantial modeling change to the code was the addition of a tapered beam option. A new analysis option was added for stacks. Within this module the stack design is subjected to an extensive dynamic and static analysis to check for compliance with the standards.

5.2 Tapered-Beam Subroutine

It is straightforward to model stacks of continuous cross sections with transfer matrices. However, many stacks are tapered or contain tapered sections, which presents a more complicated modeling problem. Ideally, a new transfer matrix would be derived for modeling continuously linear tapered beams, including rotary inertia and shear deformation. After researching various sources for such a transfer matrix, it appeared that this type of matrix was not available. Blevins [39] shows general expressions for the

natural frequencies and mode shapes of tapered beams. However, these expressions do not give enough information to create a transfer matrix for the beam (relationships between deflection, slope, moment, and shear are required). If the differential equation of a tapered beam were used, a transfer matrix solution would be possible. Several transfer matrices for constant cross section Euler-Bernoulli beams, which neglect rotary inertia and shear deformation, are given in Pilkey [40]. This document has transfer matrices for beams of various non-uniform cross sections, but shear deformation and rotary inertia are not accounted for in any of the cases. A promising article was found that dealt with modeling a tapered timoshenko beam by use of transfer matrices [13]. However, this article did not address the problem of developing a single transfer matrix for a linear tapered beam. This article instead focused on how stepped *constant section* continuum mechanics transfer matrices could be used to model a tapered beam and how this approach converged faster than a finite element approach.

In an attempt to derive the transfer matrix for a tapered beam, the method presented in Pestel and Leckie [12] was applied to a beam where the moment, cross-sectional area, and mass per unit length were treated as variables. However, while deriving this transfer matrix for a tapered beam, several problems are encountered. This includes the fact that complicated non-linear differential equations are obtained and a characteristic equation

that quickly becomes too large to be dealt with even when symbolic processors within MATLAB® and MATHEMATICA® were utilized (see Appendix 2).

Therefore, instead of using a continuously tapered beam, it was decided to investigate the possibility of using a series of stepped continuum beam segments as an approximation to a tapered beam. The investigation would require that the static and dynamic behavior of tapered sections be analyzed to find the density of stepped sections required to produce acceptable results. In a stepped approximation to a tapered beam, a method of determining the optimum outer diameter of the stepped sections is needed. The static and dynamic behavior of the model will determine the criteria for how to create the model.

5.3 Static Considerations in Tapered-Beam Approximation

The area moment of inertia for a cylindrical beam shown in Figure 5-1 is given as:

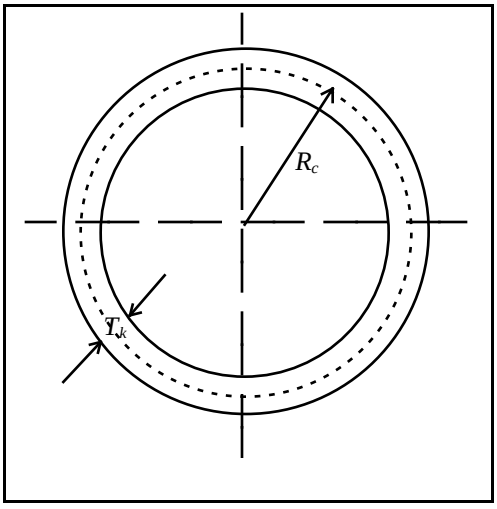

Figure 5-1. Cylindrical beam cross section.

$$I = \frac{\pi}{64}\left[(D_c + T_k)^4 - (D_c - T_k)^4\right] \tag{5.1}$$

where: $D_c = 2R_c$ = Centroidal Diameter, T_k = Wall thickness

The area moment of inertia as a function of diameter is a fourth-order polynomial. The area moment of inertia of a cylindrical beam (with a one inch (0.0254 m) wall thickness) is show in Figure 5-2 for values of D_c from 0 to 60 in (0 to 1.524 m). This curve has a fourth-order shape which clearly shows that a linear average of the outer diameters of a tapered beam will not give the correct average area moment.

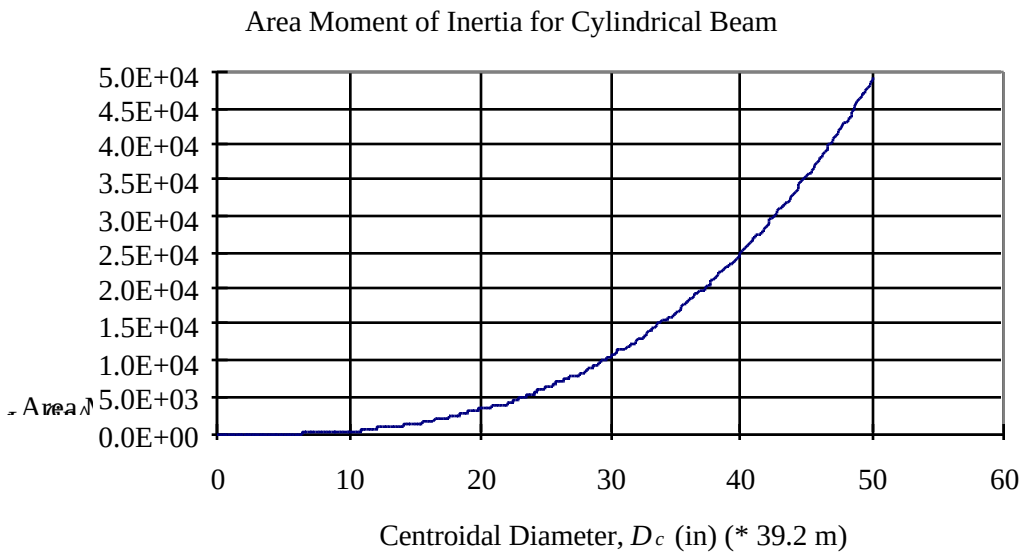

Figure 5-2. Area moment of inertia of a cylindrical beam for different centroidal diameters, and constant wall thickness of one inch (0.0254 m)

However, if the beginning and ending diameters of the tapered section are not greatly different, the moment curve begins to approximate a straight line as shown in Figure 5-3.

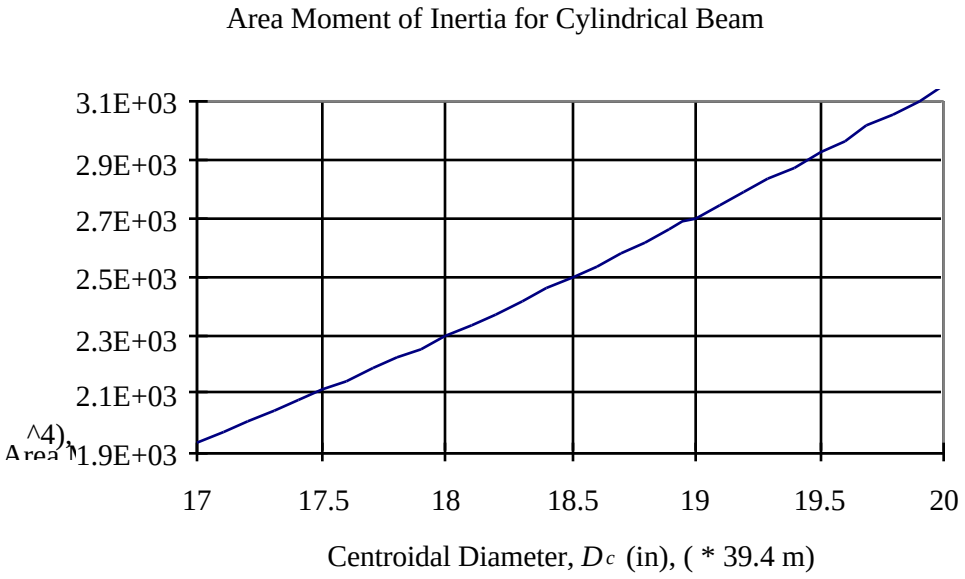

Figure 5-3. Moment of cylindrical beam, three inch (.0762 m) variation in D_c

The average area moment of a tapered section is obviously more involved than simply taking the mean diameter of the tapered section. To replace the tapered beam with a constant beam that will give the same static deflection, a means of determining the effective diameter of the constant section model is needed. To do this, the moment of the tapered section can be integrated along the tapered section and then divided by the change

in diameter, ΔD. For example, consider the beam section in Figure 5-4 that shows two constant sections joined by a tapered section.

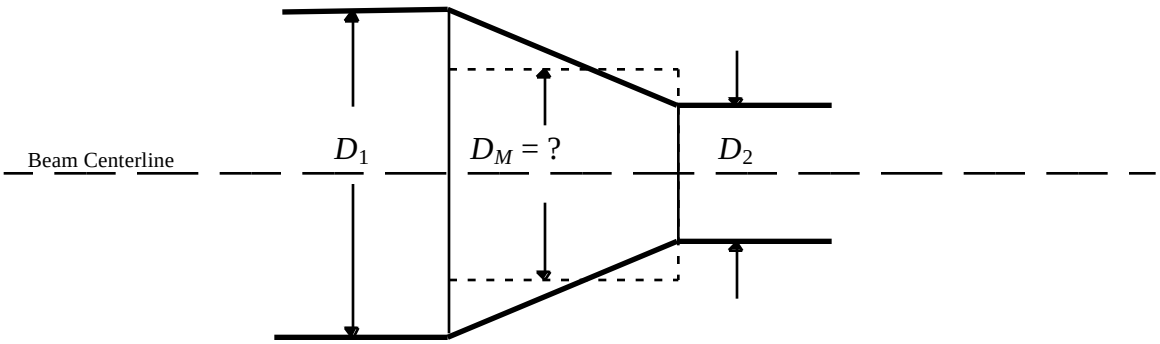

Figure 5-4. Tapered beam section joining two constant sections

In order to replace the tapered section with a constant section of diameter $D_{m,}$ a value for D_m needs to be derived. Assuming constant wall thickness, the average moment of the tapered section in Figure 5-4 is found as follows:

$$\bar{I} = \frac{1}{\Delta D} * \int_{D2}^{D1} I dD \tag{5.2}$$

$$\bar{I} = \frac{1}{D_1 - D_2} * \int_{D2}^{D1} \left[(D_c + T_k)^4 - (D_c - T_k)^4 \right] dD \tag{5.3}$$

$$\bar{I} = \frac{\pi}{64(D_1 - D_2)} \left[\frac{(D_c + T_k)^5}{5} - \frac{(D_c - T_k)^5}{5} \right]_{D2}^{D1} \text{ (assuming } D_1 > D_2) \tag{5.4}$$

$$\bar{I} = \frac{\pi}{64(D_1 - D_2)} \left\{ \left[\frac{(D_2 + T_k)^5}{5} - \frac{(D_2 - T_k)^5}{5} \right] - \left[\frac{(D_1 + T_k)^5}{5} - \frac{(D_1 - T_k)^5}{5} \right] \right\} \tag{5.5}$$

For example, consider a tapered beam for which D_1 = 20 in (0.508 m), D_2 = 17 in. (0.432 m), T_k = 1 in. (0.00254 m), and L = 50 in (1.27 m). Using the above equation for average area moment, $\bar{I}$ =150.6 in^4 (6.27 x 10^{-5} m^4). Equating this value to the moment for a constant cross section cylindrical beam with the same wall thickness, it can be found what outer diameter will give the same area moment as the tapered section:

$$\bar{I} = 2510 \text{in}^4 \ (0.00105 \text{ m}^4) = \frac{\pi}{64L}\left[(D_c + T_k)^4 - (D_c - T_k)^4\right] \tag{5.6}$$

Equation (5.6) yields D_c = 18.54 in (0.471 m). This is very close to the (linear) mean diameter of 18.5 in. (0.460 m), for which I = 2493.7 in^4 (0.00104 m^4), which is in error by only 0.65% from the actual value of 2510 in^4 (0.00105 m^4). This shows that for this case where the two diameters differ by 17%, using the mean diameter of the tapered beam would produce very little error in moment calculations.

As Figure 5-5 shows, less than ten percent error is encountered for D_1/D_2 values as high as forty, which is well beyond typical stack geometry (stacks typically have D_1/D_2 values less than ten). With such a small percent error, it would serve to use the linear average of the two diameters in the analysis program in order to expedite computation time and to save on limited memory space.

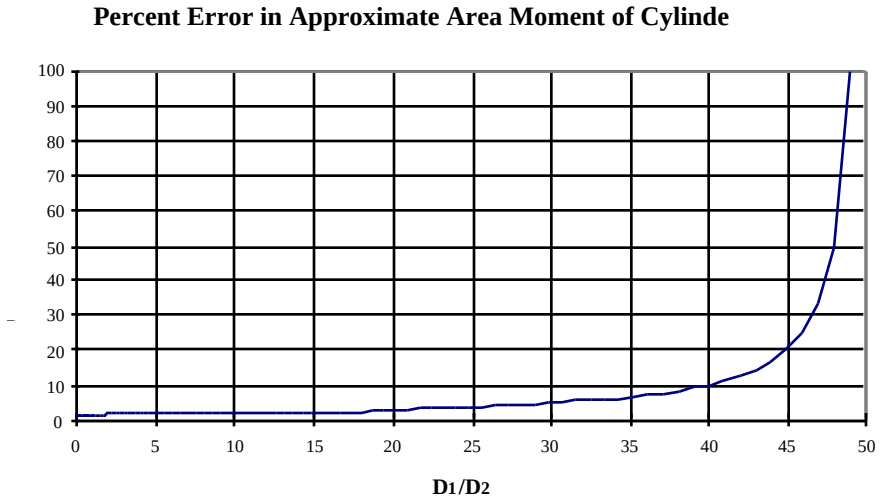

Figure 5-5. Percent error in area moment calculations of a tapered beam by replacing the tapered beam with a constant beam with the midpoint diameter

In order to determine how many stepped sections are required to obtain good dynamic results, the following study was performed.

5.4 Dynamic Considerations in Tapered Beam Approximation

In any given stack model, there are several variables which will affect how fine a mesh is required to obtain good estimates of the natural frequencies. For this study, "good" results are determined by the number of stepped sections required to get within 5% of the actual natural frequency. For computer memory limits as well as computational speed considerations, the least amount of stepped sections that will allow accurate results would be desirable. It is assumed that with an increasing number of sections to approximate the tapered beam, the natural frequencies will converge to those for a smooth tapered segment. The actual natural frequency of a tapered beam was determined by doing a convergence study on two different stack designs, design (a) and design (b).

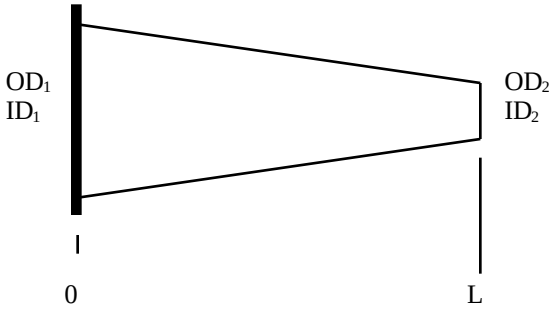

Design (a) Stack Dimensions:

L = 200 ft. = 2400 in. (60.96 m)
OD_1 = 14.5 ft. = 174 in. (4.42 m)
ID_1 = 13.5 ft. = 162 in. (4.11 m)
OD_2 = 5ft. = 60 in. (1.52 m)
ID_2 = 4.6 ft. = 55.2 in. (1.40 m)

Figure 5-6. Stack design (a) used for convergence study

Stack (a) consisted of one continuously tapered beam, with the dimensions taken from an example in the ASME Steel Stack standards [42]. This model was analyzed and eigenvalues were found using between two and thirty constant sections for the tapered approximation.

From Figures 5-7a, 5-7b, and 5-7c, it can be seen that convergence in the first three modes occurred quite rapidly, the first mode converged to within 5% of its final value after six segments were used. Only the first three modes were investigated, because this is where the greatest deflection amplitudes will occur, and all aerodynamic excitation forces are typically very low frequency.

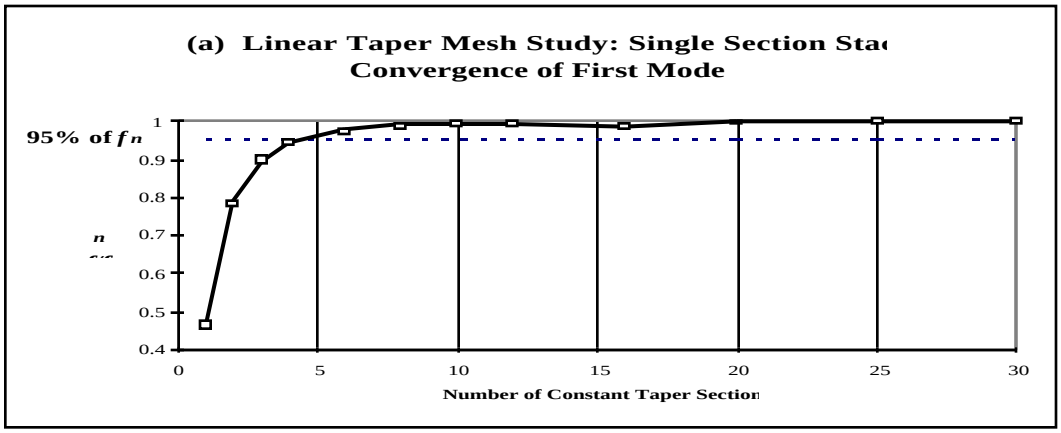

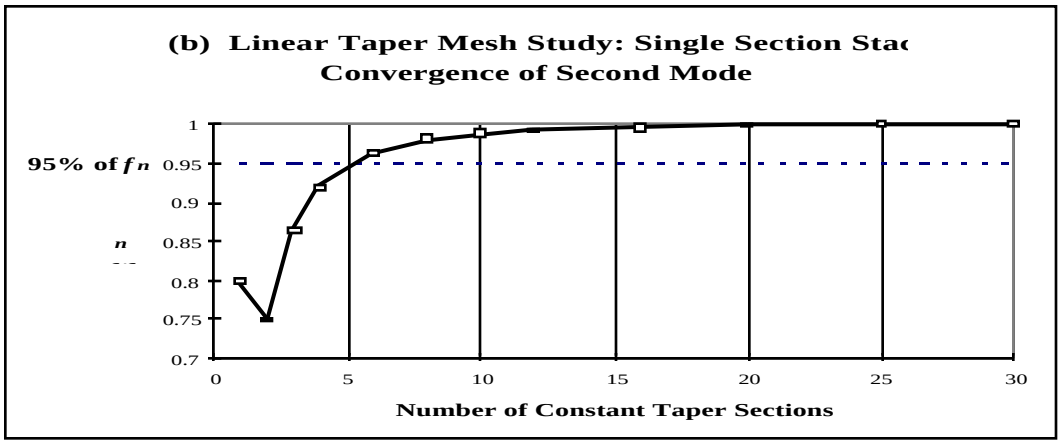

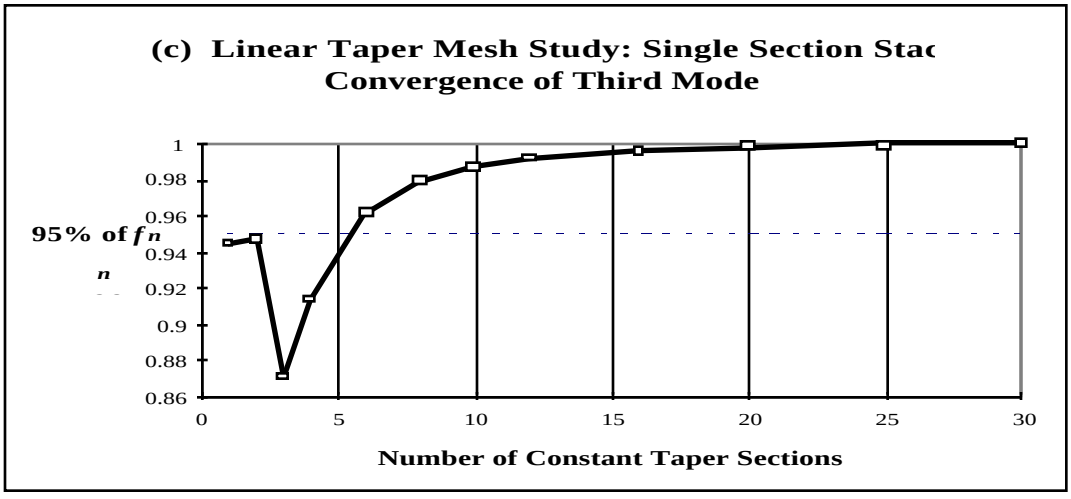

Figures 5-7. Convergence of eigenvalues for stack (a)

A different stack design was used in the second convergence study. Stack design (b) consists of two constant sections joined by a tapered section as shown in Figure 5-8. The tapered section is only about 4% of the total length of the stack, as opposed to design (a), which was 100% tapered section. This design will give an idea of how important the number of tapered sections is in the dynamics of a beam consisting largely of constant sections.

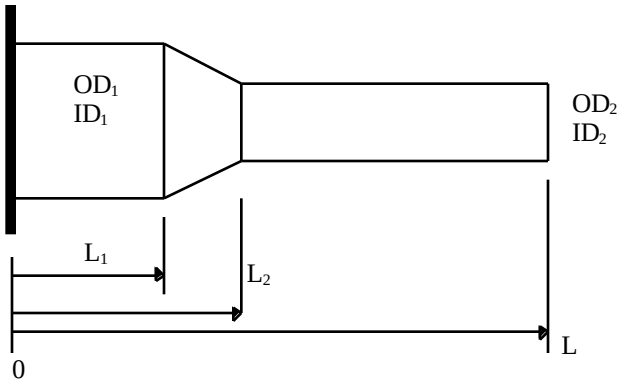

Design (b) Stack Dimensions:

L = 132 ft. = 1584 in. (40.23 m)
L_1 = 27.3 ft. = 328 in. (8.33 m)
L_2 = 32.3 ft. = 388 in. (9.86 m)
OD_1 = 7.7 ft. = 92 in. (2.34 m)
ID_1 = 7.6 ft. = 91 in. (2.31 m)
OD_2 = 5ft. = 60 in. (1.52 m)
ID_2 = 4.9 ft. = 59 in. (1.50 m)

Figure 5-8. Stack design (b) used for convergence study

Stack (b) was modeled and eigenvalues were found using between two and ten constant sections to model the tapered section. From Figures 5-9a, 5-9b, and 5-9c, it can be seen that the first three modes converged much more rapidly than those of stack (a), the first mode converged to within 5% of its final value after only one intermediate section was used.

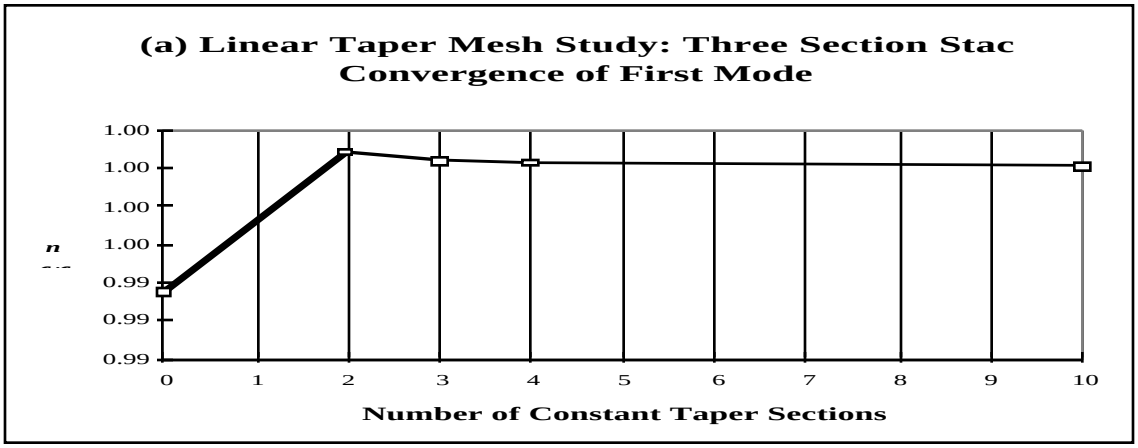

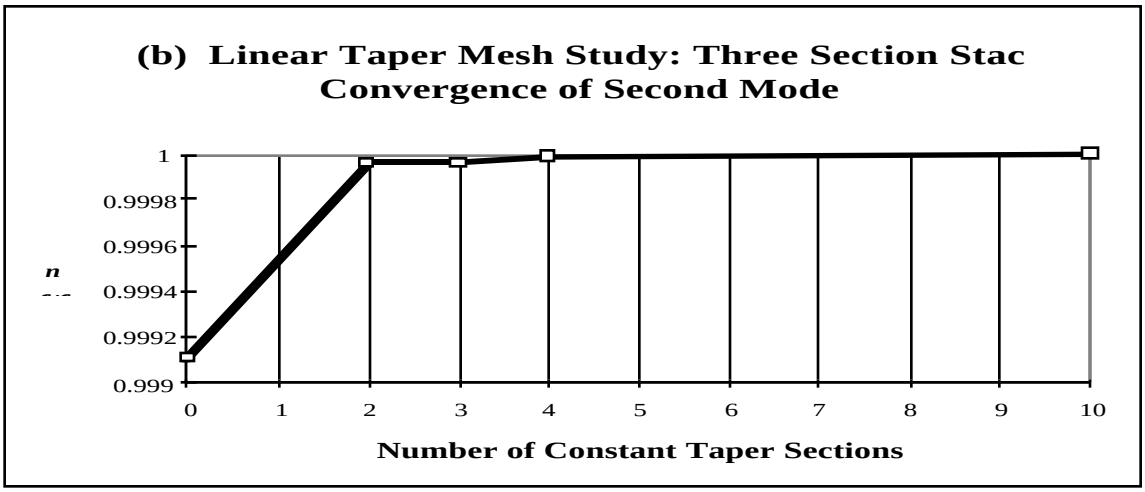

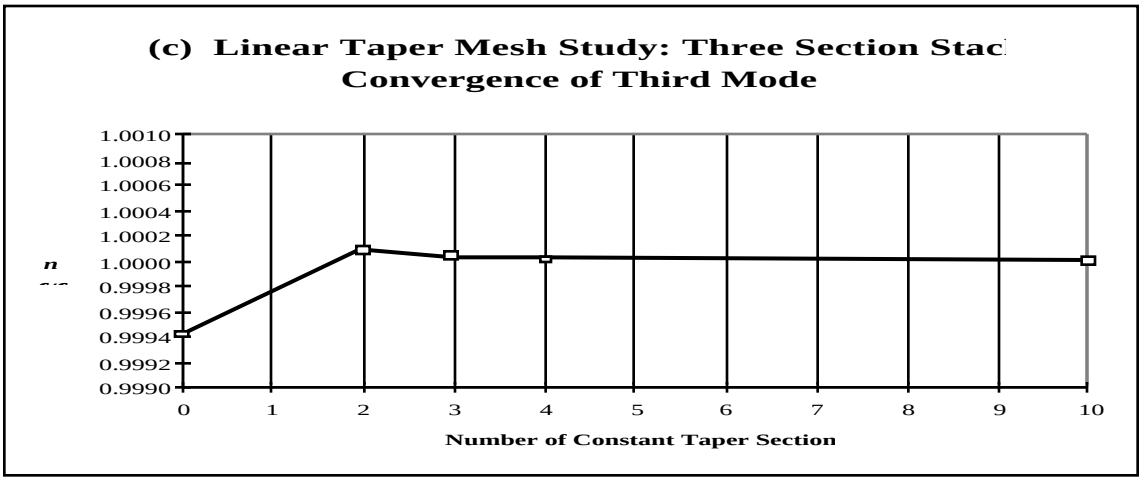

Figures 5-9. Convergence of eigenvalues for stack (b)

Because stack (b) converged much faster than stack (a), this suggests that the greater percent of the stack that is tapered, the greater the number of sections are required to obtain convergence of the modes. It appears that the worst case scenario for modeling a stack will be that of one long, tapered section with no constant sections, as seen in design (a). Therefore, because convergence for stack (a) was achieved after six sections, a stack model using ten sections should always provide accurate dynamic results. The effects of taper angle will now be studied to gain more insight into how different geometry affects convergence of the modes.

5.5 Effects of Taper Angle on Beam Dynamics

The above two example stacks give some insight as to how transfer matrices converge the natural frequencies. Other factors that need to be investigated are the effects of the taper angle, and a detailed look at the effect of changing the relative taper length. The factor that dictates the minimum number of tapered sections must be included in the analysis code.

First, in order to study the effect of the taper angle, α, was studied. The following four models were analyzed, as shown in Figures 5-10 and listed in Table 5.1. In this study, the lengths of the beam was held constant, and only the diameter of the base was varied.

Table 5.1. Stack dimensions for taper angle study

Stack	OD_1 (in)	ID_1 (in)	OD_2 (in)	ID_2 (in)	tan α	L(in)
5-10a	320	319	20	19	0.15	1000
5-10b	220	219	20	19	0.10	1000
5-10c	120	119	20	19	0.05	1000
5-10d	70	69	20	19	0.025	1000

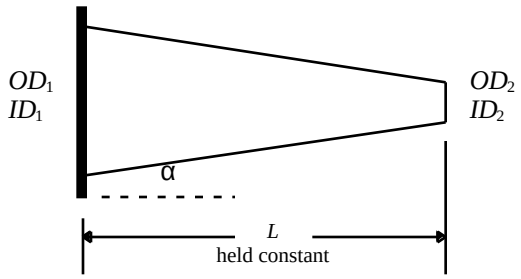

Figure 5-10. Stack model used in taper angle (α) study

Table 5.2. Convergence of natural frequencies of stacks 5-10a,b,c,d,e

Stack	Minimum # of segments to converge to within 5% of ω_n		tan α
	ω_1	ω_2	
5-10a	6	9	0.15
5-10b	6	8	0.1
5-10c	5	7	0.05
5-10d	4	5	0.025

In the above study, the maximum number of segments required to converge was $N = 9$, for the second mode when $\tan\alpha = .15$ ($\alpha = 8.5°$). This would represent a fairly abrupt taper for a stack, seeing as $\tan\alpha$ typically lies within the range of .05 to .1 on most stack designs.

5.6 Dynamic Effects of Relative Tapered Section Length

In section 5.4 it was shown that a stack with a smaller ratio of tapered section length to total stack length would converge faster. To gain a better understanding of how the tapered section length affects the accuracy of the calculated natural frequencies, various beam configurations will be tested in this section. The ratio of length of the tapered section (L_T) to length of the straight section (L_S) is the variable, and the taper angle, α, is held constant, as shown in Figure 5-11 and listed in Table 5.3.

Table 5.3. Stack dimensions for L_s/L_T study

Stack	OD_1 (in)	ID_1 (in)	OD_2 (in)	ID_2 (in)	L_S/L_T	L_s(in)	L_T (in)
5.13a	60	59	10	9	0.25	250	1250
5.13b	60	59	20	19	0.5	500	1000
5.13c	60	59	30	29	1	750	750
5.13d	60	59	40	39	2	1000	500
5.13e	60	59	56	55	14	1400	100

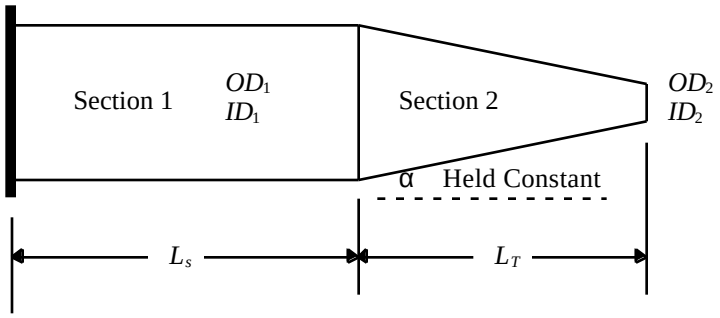

Figure 5-11. Stack design used in L_S/L_T study

Table 5.4. Convergence of natural frequencies of stacks 5.13a,b,c,d,e

Stack	Minimum # of segments to converge to within 5% of ω_n		L_s/L_T
	ω_1	ω_2	
5.13a	5	6	0.25
5.13b	3	3	0.5
5.13c	2	2	1.0
5.13d	1	1	2.0
5.13e	1	1	14.0

In this study of the effect of L_s/L_T was studied in detail over a wide range of designs. The limiting case was found to be with stack 5.13a, mode #2. This design required a minimum of six sections to converge.

Considering the two studies, the effect of α and the effect of L_s/L_T, the maximum number of segments required for convergence was $N = 9$. All typical stack designs should fall well within the bounds of these two studies. In order to encompass all of the above possible

stack configurations, however, the STACK1 code will default to N = 10 segments per tapered section in order to ensure accurate dynamic results.

5.7 Implementation of Tapered Beam Routine

When considering various stack parameters such as α, L_S/L_T, static deflection and modal convergence while using the transfer matrix method, it appears that when considering all possible stack configurations, the maximum number of mesh sections needed to model a tapered section is N = 9. Therefore, a value of N = 10 sections per tapered beam will be set as the default in the beam program.

Because it has been shown adequate to model the stepped sections with the average diameter along a given segment, the following method is used to mesh tapered beam sections. First, the user is prompted for the beginning and ending inner and outer diameters and section length. Then an automatic mesh generator loops through the transfer matrix code and creates a series of stepped beams to model the tapered section. The beginning and ending wall thickness do not have to be the same, for the mesh generator will automatically linearly interpolate between the two thicknesses. For example, if a tapered section is being modeled to join a larger diameter section with a smaller diameter section, the mesh would appear as shown in Figure 5-12 (with N=3 for clarity):

Figure 5-12 shows only the half of the stack section. In this type of taper, the first taper section is already reduced in diameter, in order for the real taper line (represented by the dashed lines) to pass through the midpoint of the section. The same is true for the final taper section, in that it is slightly larger in diameter than the following constant section in order to maintain the correct average moment.

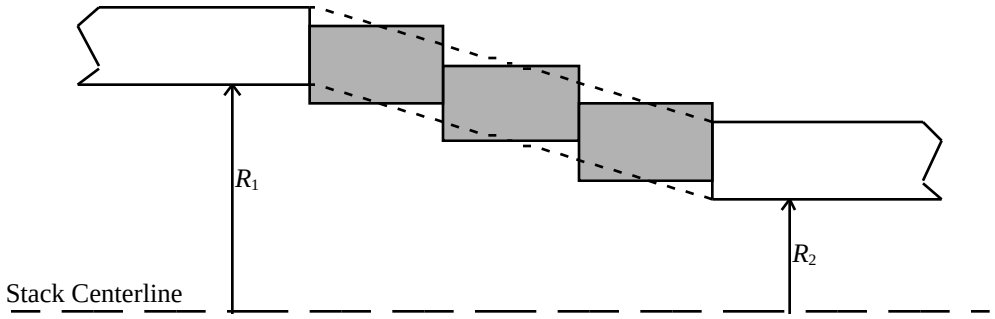

Figure 5-12. Example of automatic mesh routine

5.8 Implementation of ASME Steel Stack Standards Into STACK1 Code

Now that an efficient stack modeling procedure is available, the next step is to check the stack design against the standards to obtain various static and dynamic information that can be used to check and improve the stack designs. Various items, including stack natural frequencies, geometry, wind exposure category (dependent on surrounding structures), and geographic location (which determines maximum wind velocity) are required to completely study the behavior of a given stack design. Care should be taken

to accurately describe each aspect of the stack model. Boundary conditions should be applied carefully. A fixed-free approach is appropriate when the stack is mounted on bedrock. If the stack is mounted on a building or on a soft foundation, the correct boundary conditions must be applied. In addition to boundary conditions, the modeler must use an accurate value of structural damping in order to obtain valid dynamic data. Although the small damping value present in welded steel stacks does not play much part in determining the natural frequencies, rather, it is an important factor in determining the gust response factor. Steel stacks have relatively low inherent structural damping. The damping value is not only dependent on material properties, but also method of construction. For example, an all-welded stack will have lower damping than an all-bolted stack. Additional damping is gained from other structural features such as a lining, soil foundation interaction, and aerodynamic forces, the latter of which may actually reduce the damping [18]. A table of observed damping values for stacks has been tabulated in the ASME steel stack standards [27].

Table 5.5. Representative Damping Values. Percent of Critical Damping, adapted from ASME standards [27]

	----------DAMPING VALUE ----------		
Welded Stack	Low	Average	High
Unlined	0.0016	0.004	0.006
Lined	0.0032	0.0067	0.010

The damping values in the above table are given in terms of the fraction of critical damping β which is related to the logarithmic decrement δ by the relationship $\delta = 2\pi\beta$ [27].

5.9 Static Loads and Deflection

Once the correct modeling procedures have been followed, the wind loads on the stack are applied. The first step in doing this is realizing the geographic location of the stack. The location dictates the corresponding basic design wind speed from the standards, as shown in Chapter 3. The basic design speed (V_R) is the "fastest mile" wind speed at a height of 33 ft (10.1 m). over open terrain having a return period of 50 years. V_R is defined in miles per hour [27].

After selecting a value for V_R, the velocity pressure exposure coefficient, K_z is determined. K_z is a function of exposure category and height above ground level. Exposure categories are defined as in Table 5-6.

Table 5.6. Exposure categories, adapted from ASME standards [43]

Exposure Category	Brief Description
A	Large city centers with at least 50% of the buildings having a height of 70 ft.
B	Urban and suburban areas, wooded areas, or other terrain with numerous closely spaced obstructions having the size of single family dwellings or larger
C	Open terrain with scattered obstructions having height generally less than 30 ft
D	Flat, unobstructed coastal areas directly exposed to wind flow over large bodies of water or very exposed areas on hills

After selecting an exposure category, the standards provide a table of velocity pressure exposure coefficients (K_z) as a function of height above the ground. Now that the basic design speed (V_R) and K_z have been selected, the velocity pressure q_z (lbf/ft^2) can be calculated by the following:

$$q_z = 0.00256\, K_z (V_R)^2 \ \text{lbf/ft}^2 \tag{5.7}$$

To get a better idea of how the velocity pressure varies with exposure category and height above ground level, consider Figure 5-13 which shows the velocity pressure for Blacksburg, Virginia (for which V_R = 70 mph (31.3 m/s).

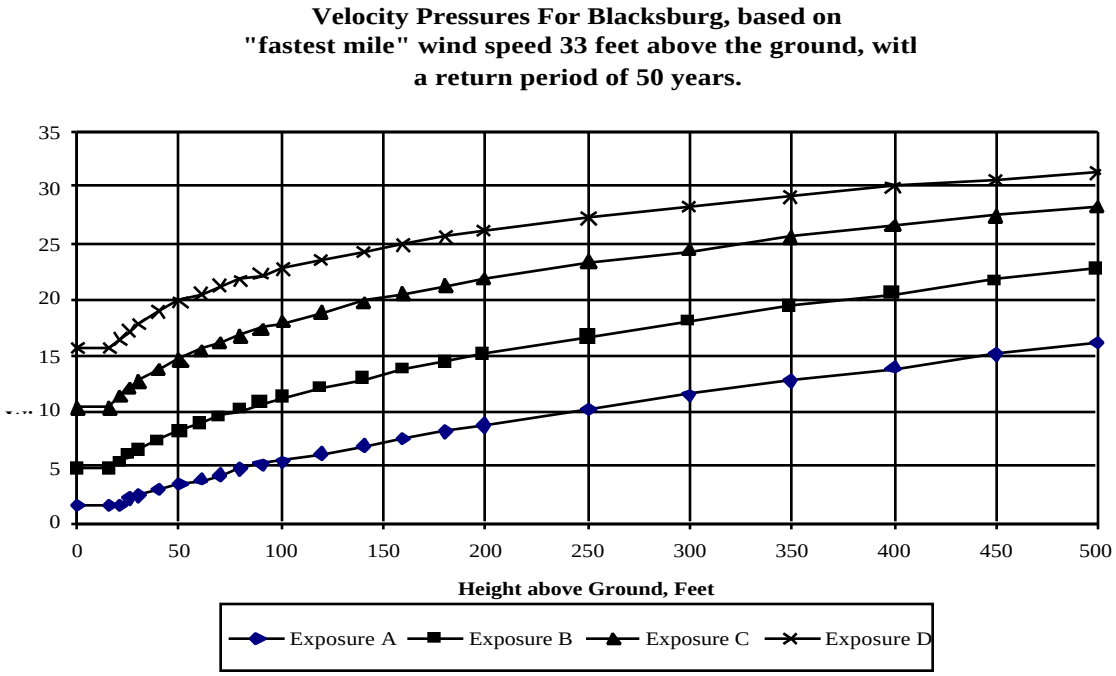

Figure 5-13. Velocity pressures for Blacksburg, Virginia

The next step in calculating wind load is to determine the gust response factor, $\overline{G}$, after the ASME standards [27].

$$\overline{G} = .65 + \left[\frac{P}{b} \frac{(3.32 T_1)^2}{1 + .002 D} \right]^{1/2} \qquad (5.8)$$

(see Appendix 1 for full discussion of all variables and calculations)

The above expression for $\overline{G}$ is taken from the 1992 ASME Steel Stack Standards [27]. A more updated ASCE building code suggests that values of $\overline{G}$ can be approximated by a simplified method which does not require many of the constants contained in the ASME equations. The above ASME procedure is a valid analysis, but, for simplicity's sake within the STACK1 code, the more recent ASCE code is used.

Finally, the load per unit height of the stack is given by:

$$W_z = C_f q_z D G \text{ (lb / ft)} \qquad (5.9)$$

where: C_f = a force coefficient given in table 5.C-1 of the ASME standards [49],

q_z = velocity pressure from eqn. 5.7, D = diameter of stack at $0.8H$, and

G = gust response factor from eqn. 5.8.

(see appendix 1 for full discussion of all variables and calculations)

In the code, the value for W_z is determined at the beginning and end of each beam section. STACK1 then determines static deflection based on this velocity pressure, as well as internal shear, moment, and stresses.

5.10 Dynamic Loads and Vortex Shedding

Once the static load is known, the next step is to determine the dynamic behavior of the stack. The mean hourly design speed, V_D is defined as:

$$V_D(z) = 1.18 V_R \sqrt{K_z} \quad ; \text{where } z = 5/6\ H \tag{5.10}$$

The critical wind speed, in feet per second, is given by:

$$V_c = f_1 d / S_t \tag{5.11}$$

where: f_1 = the first natural frequency, d = mean diameter of upper one-third of stack, ft., S_t = Strouhal number, usually used as .2 for single stacks, and may vary due to Reynolds numbers and multiple

stacks [27]

If $V_c > 1.3\ V_D$, then no vortex shedding consideration is required. If this is not the case, the following steps shall be used, after the ASME standards [27].

(A) Calculate m^1, a constant used in the standards to calculate the dynamic response, (see Appendix 1)

(B) If $m^1 < .4$, large amplitude motions (tip deflections of $.4d$ to $1.0d$) are probable.

(C) If $.4 < m^1 < .8$, large amplitude motions, up to $.4d$, are possible.

(D) If $m^1 > .8$ and $V_c > .4V_D$, then across wind motion in the fundamental mode is not significant. If $V_c < .4V_D$ then across wind motion for the second mode should be calculated and checked [27].

The STACK1 code will automatically advise the user as to what type of vortex induced motion should be expected, as well as what types of tip deflections can be expected. The following chapter shows how this process works on two example stacks.

Chapter 6: Test Examples

6.1 ASME Example Stack

The following example stack was taken from the ASME Steel Stack Standards [42]. The stack consists of a single 200 ft (60.1 m) tapered section that changes from 166 in (4.20 m) outer diameter at the base to 60 in (1.52 m) outer diameter at the top. The wall thickness also changes along the stack, from 1.5 in (0.04 m) at the base to .5 in (0.01 m) at the top.

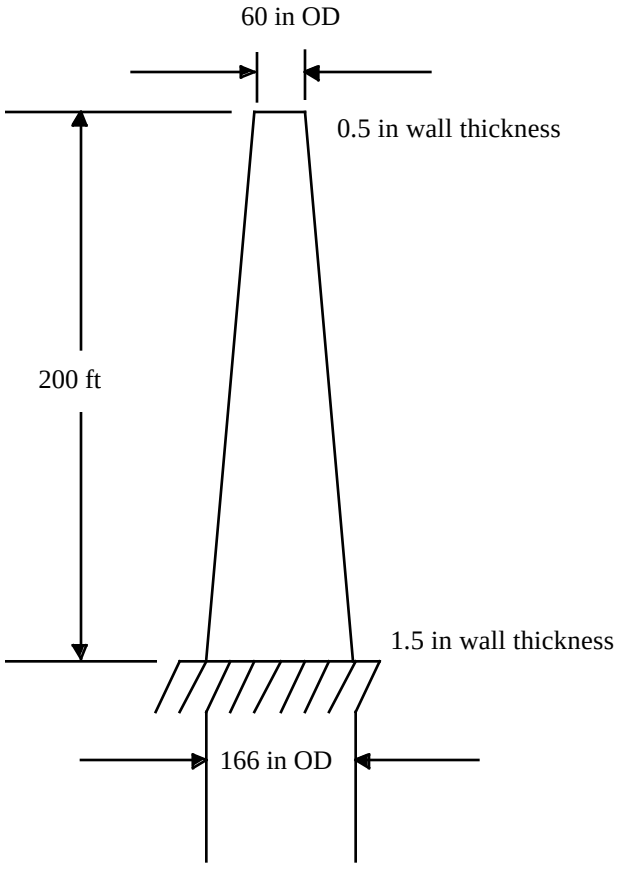

Figure 6-1. ASME example Stack geometry [42]

The STACK1 code was used to model the geometry by using ten discrete sections. The code automatically accounts for the change in wall thickness by linearly interpolating this dimension for each of the segments.

The basic design speed, V_R, was chosen as 100 mph, and the exposure category was set to "C".

STACK1 found the results tabulated in Table 6.1.

Table 6.1. STACK1 Results of Figure 6-1 Example

First natural frequency, f_1	1.81 Hz
Second natural frequency, f_2	6.46 Hz
Third natural frequency, f_3	15.00 Hz
Maximum load per unit height, W_Z	316.34 lb / in
Mean hourly design speed, V_D	100.0 mph
Critical design speed, V_C	66.1 mph

From the above results, it can be seen that $V_c < 1.3\, V_D$. The ASME standards describe this as a situation where vortex shedding is a concern [27]. Because of this, STACK1 continues to follow the ASME procedure by calculating a dimensionless deflection parameter, m^1, which essentially gives the magnitude of stack tip deflection.

In this case, $m^1 = 17.7$, for which the standards dictate that large amplitude motions of up to $.4d$ are possible, with d being the mean diameter of the upper one-third of the stack.

Figure 6-2 on the following page shows the stack model with the applied static loads. The static deflection curves are shown in Figure 6-3, which represents the deflections that will occur when the stack is exposed to 100 mph winds.

The model set-up in Figure 6-2 shows how STACK1 uses stepped constant sections to approximate the continuous taper. The static wind loads are represented by the arrows on the side of the stack. The length of these arrow shows the intensity of the velocity pressure at a given height. From Figure 6-3, the tip deflection will be around 15 in (.38) under the given wind conditions.

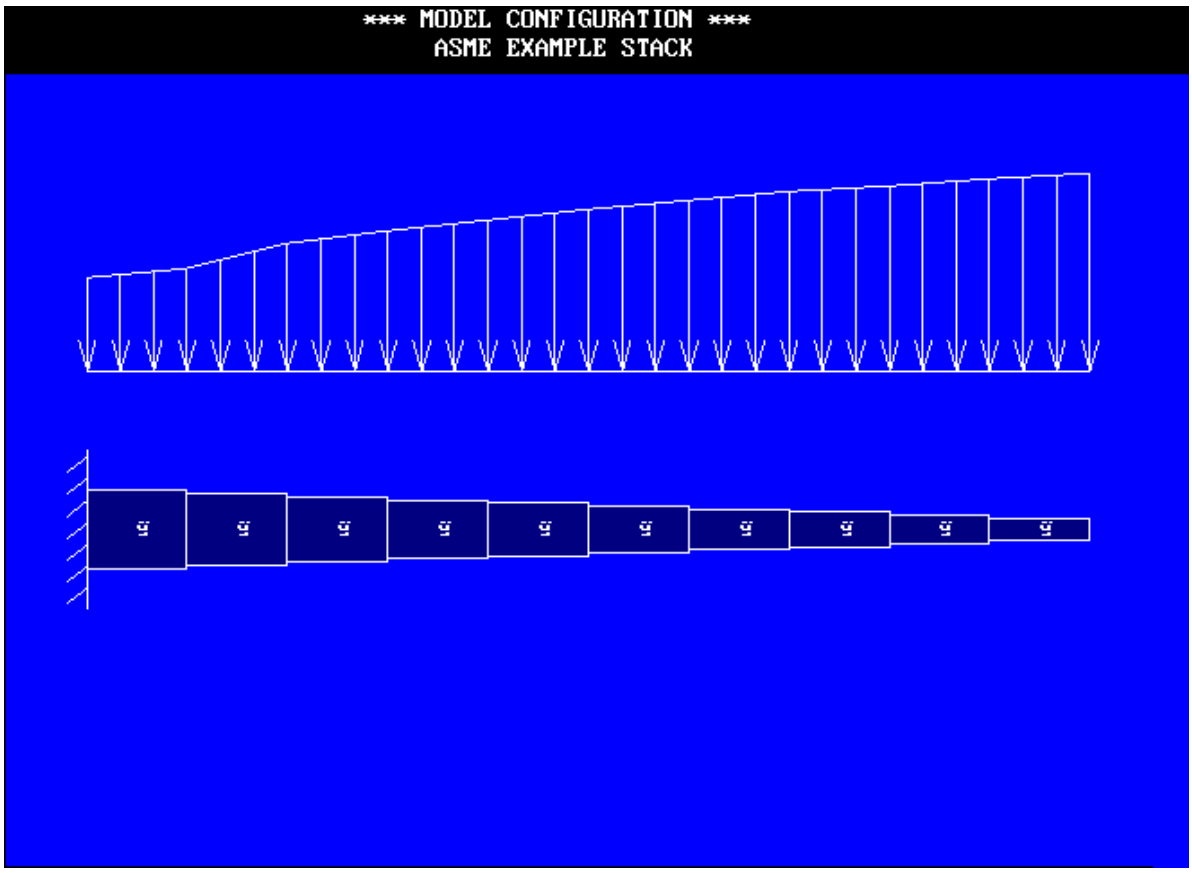

Figure 6-3. Model geometry within STACK1 (ASME example smoke stack)

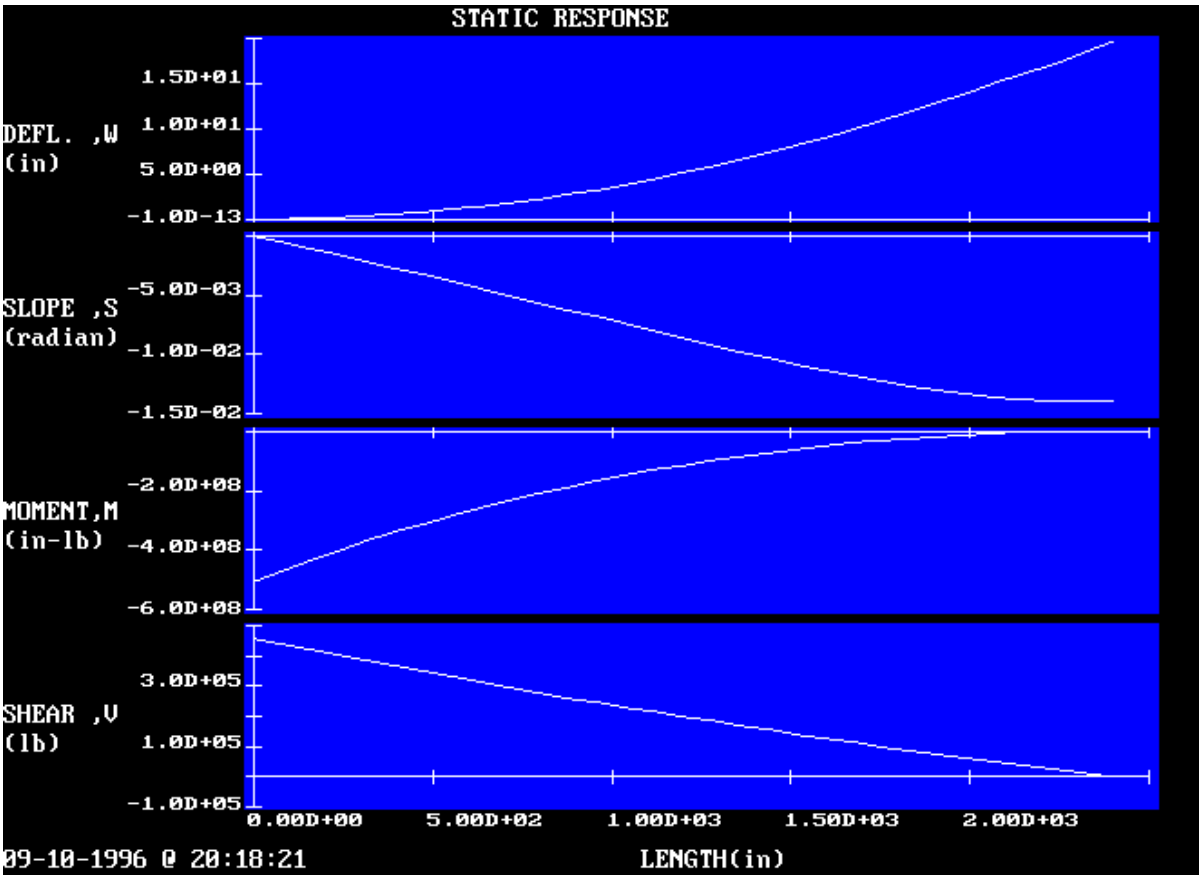

Figure 6-4. Static deflection, slope, moment and shear graphs for example 1

6.2 DUPONT Example Stack

The following example stack was taken from plans provided by DuPont. This design is more complicated than the example demonstrated in section 6.1. This stack exploits the tapered section option within STACK1, which provides the decreasing diameter taper and the increasing diameter taper. The geometry of the four constant diameter sections and three tapered sections are shown in Figure 6-4. The exposure category for this example is "C", and the basic design wind speed is 100 mph.

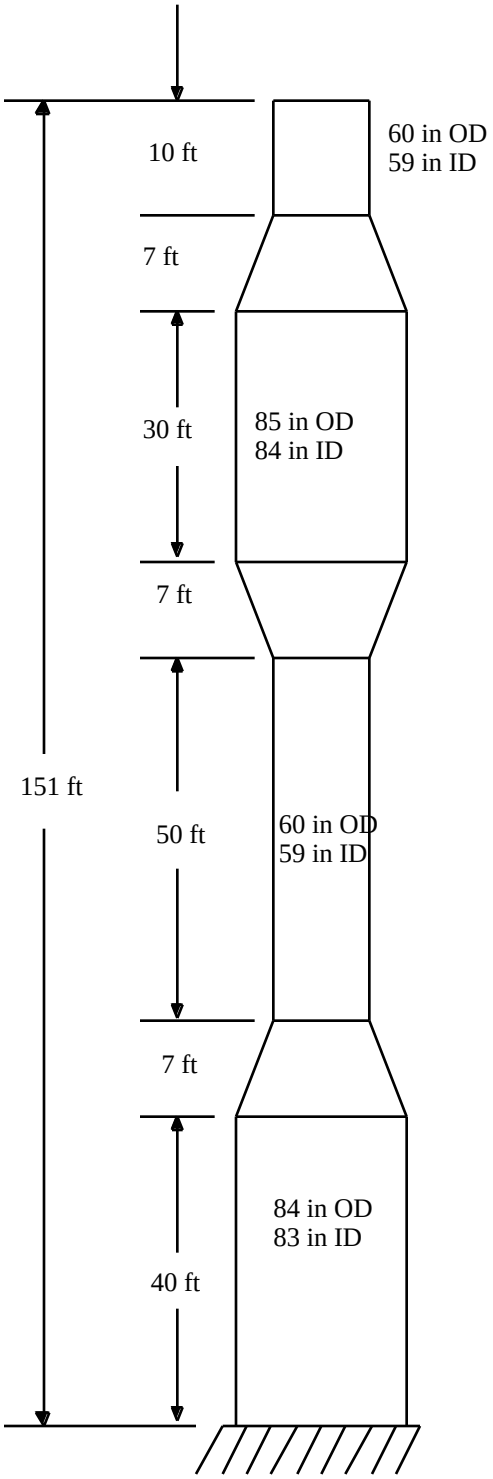

Figure 6-4. DuPont example smoke stack geometry

The STACK1 code was used to model the geometry by using various tapered and constant sections. In this case, the tapered sections were modeled with five segments in order to meet system memory requirements. The wall thickness of this stack is constant throughout.

STACK1 found the results tabulated in Table 6.1.

Table 6.2. STACK1 Results of Figure 6-4 Example

First natural frequency, f_1	1.03 Hz
Second natural frequency, f_2	6.09 Hz
Third natural frequency, f_3	17.23 Hz
Maximum load per unit height, W_Z	66.56 lb / in
Mean hourly design speed, V_D	100.0 mph
Critical design speed, V_C	31.12 mph

From the above results, it can be seen that $V_c < 1.3\, V_D$. The ASME standards describe this situation as similar to example 6-1, in that vortex shedding is a concern [27]. Because of this, STACK1 continues to follow the ASME procedure by calculating a dimensionless deflection parameter, m^1, which essentially gives the magnitude of stack tip deflection. In this case, $m^1 = 11.7$, for which the standards dictate that large amplitude motions of up to $.4d$ are possible, with d being the mean diameter of the upper one-third of the stack.

Figure 6-5 on the following page shows the stack model with the applied static loads. The static deflection curves are shown in Figure 6-6, which represents the deflections that will occur when the stack is exposed to 100 mph winds.

The model set-up in Figure 6-5 shows how the multiple tapered and constant sections are configured by STACK1. The static wind loads are represented by the arrows on the side of the stack. From Figure 6-6, the tip deflection will be around 40 in (1.02) under the given wind conditions.

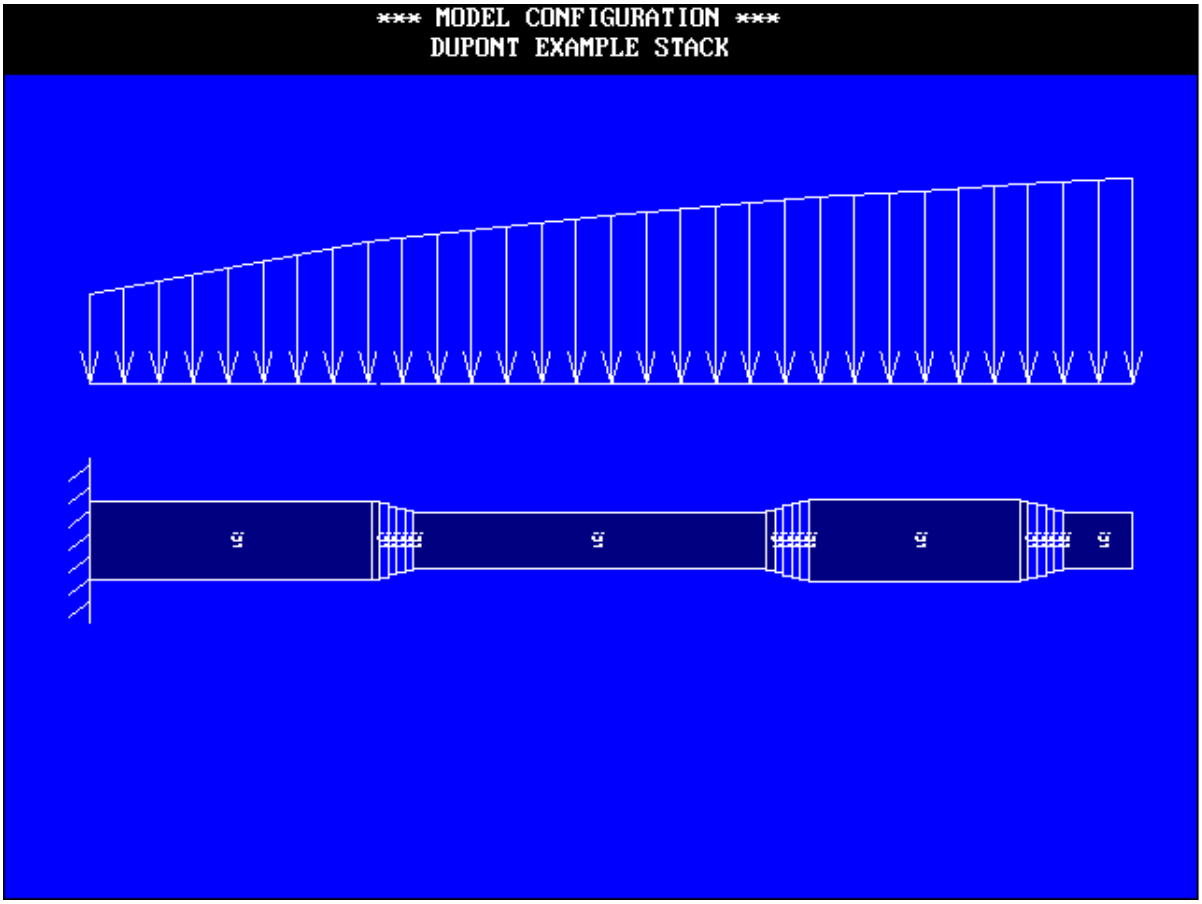

Figure 6-6. Model geometry within STACK1 for DUPONT example smoke stack

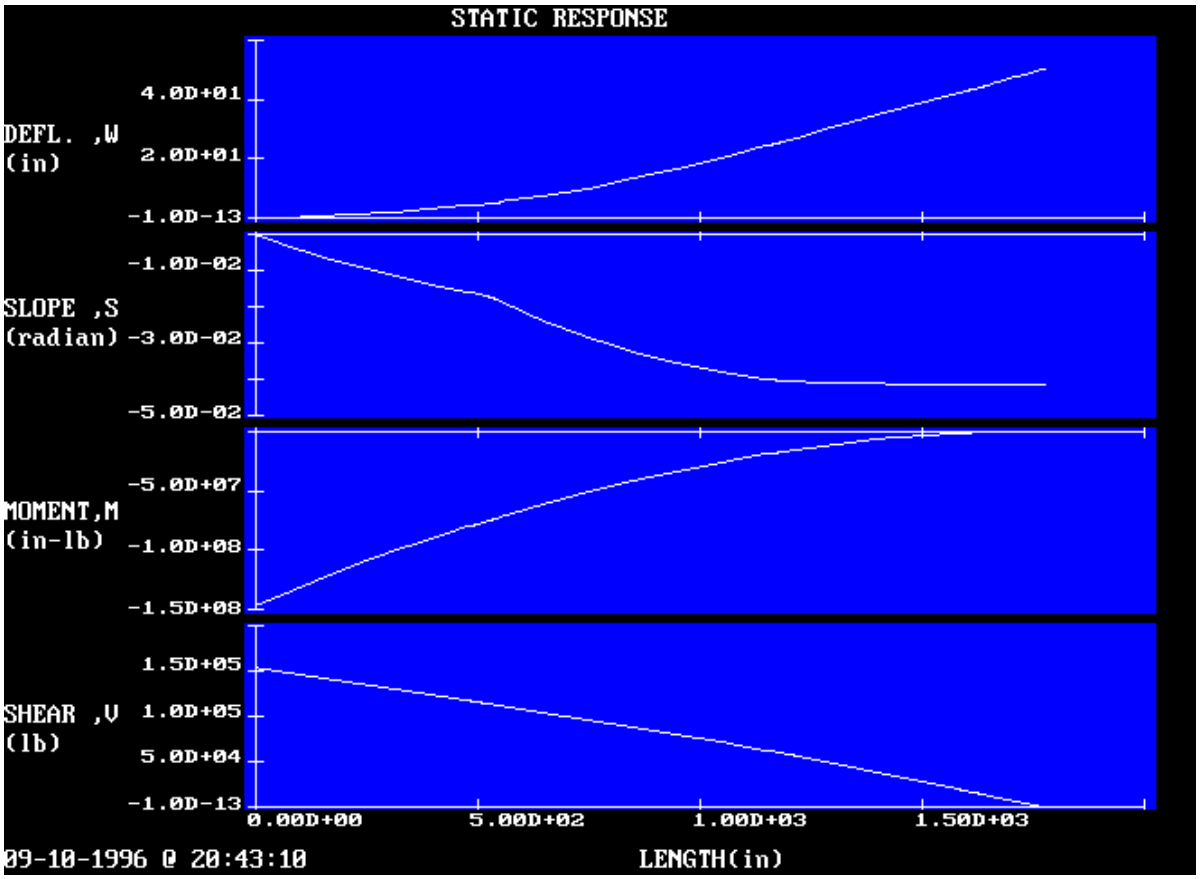

Figure 6-7. Static deflection, slope, moment and shear graphs for example 2

Chapter 7: Conclusions and Recommendations

7.1 Conclusions

In this research, the process of analyzing a steel smoke stack subject to wind loads was studied in detail. The interaction of various aerodynamic forces such as static drag loads and harmonic excitation by vortex shedding and atmospheric turbulence was studied in detail. Vibrations in the along-wind direction as well as the across-wind direction were studied, and the amplitudes of the vibration was predicted.

A computer program, STACK1, was developed which utilizes the transfer matrix method. Many features to suit the stack analyst were incorporated in this code. First, a automatic tapered beam generator was added to the code. Extensive studies were performed to validate the method of modeling a tapered beam. Second, a complete static and dynamic analysis was implemented to check the codes against the ASME Steel Stack Standards [2]. Information regarding the static deflection and maximum vibration amplitudes are provided to the user to expedite the design process.

7.2 Recommendations

To follow up on the research begun here, the following recommendations are suggested:

- Only bending vibration is treated in STACK1. Other modes of vibration, such as axial and/or ovalling are typically concerns of stack designers as well. These should be added to STACK1 to analyze stacks in more detail.
- The possibility of adding guy wires, stiffener rings, or other structural features would facilitate a more accurate analysis of some stack designs.
- If possible, the operating platform of the STACK1 program should be upgraded from DOS to WINDOWS 95®, which would not only allow the program to grow beyond the 640K memory barrier, but would also allow program debugging to take place immensely faster than the current setup.
- A post processing module for analyzing the stresses could be implemented which would include an option for fatigue analysis.

REFERENCES

1. Blevins, Robert D., *Flow Induced Vibration,*Van Nostrand Reinhold, New York, 1990, New York, New York, p. 78.
2. American Society of Mechanical Engineers, *Steel Stacks ASME STS-1-1992*, American Society of Mechanical Engineers, 1993, p. 24.
3. Reference 2, p. 46.
4. Reference 2, p. 1.
5. Reference 2, p. iii.
6. American Society of Civil Engineers, *Minimum Design Loads For Buildings and Other Structures,* American Society of Civil Engineers, New York, New York, 1995, p. 159.
7. American Society of Civil Engineers, *Wind Loading and Wind-Induced Structural Response,* American Society of Civil Engineers, 1987.
8. Reference 7, p. 117.
9. Asawa, G. L.and Garde, R.J., "Atmospheric Boundary Layer and Its Simulation in Wind Tunnels", *Wind Loads on Structures*, 1991, pp. 21-37.
10. Vickery, B.J., "Wind Loads On Towers and Chimneys", *Wind Loads on Structures*, 1991, pp. 87-100.
11. Reference 1, pp. 43-85.
12. Pestel, E. and Leckie, F., *Matrix Methods in Elastomechanics,* McGraw-Hill, New

York, 1963.

13. Shen, Ji Yao, "Continuous Dynamic Model for Tapered Beam-Like Structures," *Journal of Aerospace Engineering*, Vol. 7, October 1994, pp.435-445.
14. Reference 2, p. 87.
15. Cermak, Jack E, "Atmospheric Boundary Layer Modelling in Wind Tunnels," *Wind Loads on Structures*, 1991, pp. 3-20.
16. Reference 15, p. 5.
17. Lin, Y. K., "Structural Response Under Turbulent Flow Excitations," *Random Excitation of Structures by Earthquakes and Atmospheric Turbulence*, CISM, Udine, New York, 1977, p. 265.
18. Reference 2, p. 21.
19. Reference 17, p. 306.
20. Reference 17, p. 266.
21. Reference 1, p.1.
22. Reference 1, p. 36.
23. Kreith, Frank and Bohn, Mark S., *Principles of Heat Transfer*, West Publishing Company, St. Paul, MN, 1993.
24. Reference 1, p. 44.
25. Reference 7, p. 118.

26. Reference 2, p. 79.

27. Reference 2, p. 22.

28. Reference 10, p. 89.

29. Reference 1, p. 47.

30. Reference 12, p. vii.

31. Reference 12, p. 53.

32. Reference 12, p. 51.

33. Reference 12, p. 57.

34. Reference 12, p. 58.

35. Reference 12, p. 59.

36. Reference 12, p. 60.

37. Reference 12, p. 82.

38. Reference 12, p.86.

39. Blevins, Robert D., *Formulas for Natural Frequency and Mode Shape*, Van Nostrand Reinhold Company Inc., New York, 1979.

40. Pilkey, W. D., *Manual for the Response of Structural Members Volume II,* Engineering Mechanics Division, IIT Research Institute, Chicago, p. III113.

41. Reference 12, pp. 132-137.

42. Reference 2, pp. 70-71.

43. Reference 2, p. 91.

44. Reference 2, p. 90.
45. Reference 2, p. 84.
46. Reference 2, p. 85.
47. Reference 2, p. 86.
48. Reference 2, p. 91.
49. Reference 2, p. 89.
50. Reference 12, p. 130.
51. Reference 12, p.133.
52. Reference 2, p. 78.
53. Reference 12, p. 134.

Appendix I: STACK EXAMPLE TO VERIFY CODE

The following example stack shown in Figure A.I-1 is analyzed by following the ASME STS-1-1992 STEEL STACK STANDARDS [27].

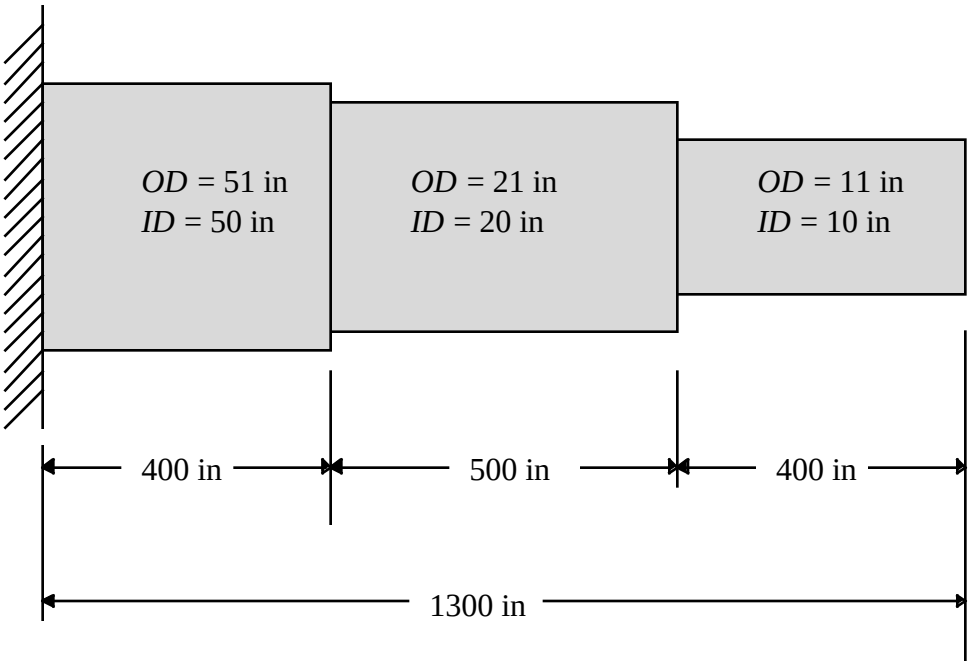

Figure A.I-1. Example stack used for calculations

For this model:

Modulus, $E = 30 \times 10^6$ in^4

Structural damping factor, $\xi_E = .05$

Shear modulus, $G = 11.5 \times 10^6$ psi

Shear Damping factor, $\xi_G = .05$

Material density, $\rho = 0.243$ lb/in^3

Exposure Category "C"

Basic Design Speed, $V_r = 100$ MPH

Equations used from ASME standards:

Velocity pressure, $q_z = 0.00256\, K_z\, (V_R)^2$ (A1.1)

where:

K_z is provided by the standards [44]

Gust response factor, $\overline{G} = 0.65 + \left[\beta \frac{P}{1 + 0.002D} (3.32T_1)^2\right]^{1/2}$ (A1.2)

Where:

$P = \bar{f} JY$ (A1.2a)

$\bar{f} = 10.5 f_1 H/(sV_R)$ (A1.2b)

J is provided by the standards [45]

Y is provided by the standards [46]

f_1 = the first natural frequency of the stack

β = structural damping as a fraction of critical

S provided by the standards [47]

s provided by the standards [48]

H = total height of stack, ft.

D = diameter of stack at .8 H, ft.

V_R = Basic Design Speed, mph

$$T_1 = 2.35\ (D_o)^{1/2} / (z/30)^{1/\alpha} \qquad \text{(A1.3)}$$

where:

$$z = 2/3\ H \qquad \text{(A1.3a)}$$

α is provided by the standards [48]

D_o is provided by the standards [48]

$$\text{Load per unit height, } W_z = C_f\, q_z\, D\, \overline{G} \qquad \text{(A1.4)}$$

where:

C_f = a force coefficient provided by the standards [49]

Vortex shedding calculations:

$$\text{Mean hourly design speed: } V_D(z) = 1.18\ V_R\ (K_z)^{1/2} \qquad \text{(A1.5)}$$

Where:

$$z = 2/3\ H \qquad \text{(A1.6)}$$

Critical Wind speed: $V_c = f_1\ d / S_t$ (A1.7)

where:

d = mean outer diameter of upper one-third of stack, ft.

S_t = Strouhal number, ususall used as 0.2 for single stacks,

but may very due to Reynolds numbers and multiple stacks.

If $V_c > 1.3\ V_D$ then NO vortex shedding consideration is requrired.

<u>Otherwise; calculate the following:</u>

$$m^1 = m\beta / \phi d^2 \qquad \text{(A1.8)}$$

Where:

m = average mass per unit length for top one-third of stack, lb/ft

β = structural damping as a fraction of critical

ϕ = air density, lb/ft^3

<u>If $m^1 < 0.4$:</u>

Large amplitude motions (tip deflections of 0.4d to 1.0d) are PROBABLE.

Use para. 5.4 ASME Standards [2] to suppress large motions.

If $0.4 < m^1 < 0.8$:

Large amplitude motions, up to 0.4d, are possible.

If unacceptable with respect to fatigue problem,

use para. 5.4 ASME Standards [2] to suppress large motions or

achieve $V_c > 1.3\ V_d$

If $m^1 > 0.8$ AND $V_c > 0.4V_D$

Stresses induced by shedding MAY exeed the drag load stresses.

The procedure used in Appendix 5.C ASME Standards [25] will be used.

If $m^1 > 0.8$ and $V_c > 0.4V_D$:

Across-wind motion in the fundamental mode is NOT significant.

If $Vc < 0.4\ V_D$ then across-wind motion for the second mode should be calculated and

checked by Method 2 of Appendix 5.C, ASME Standards [25].

Hand Calculations for example stack

Location #	Kz for Expos. C	Qz(lbf/ft^2)	f1 (Hz)	H (ft)	s (lower case)	J	gamma	D/H
0			1.134	108.3	1	0.005	0.00212	0.0085
1	1.03	26.368	1.134	108.3	1	0.005	0.00212	0.0085
2	1.265	32.384	1.134	108.3	1	0.005	0.00212	0.0085
3	1.42	36.352	1.134	108.3	1	0.005	0.00212	0.0085

Location #	Y	P	beta	D (ft)	d_min	f_bar	S (upr case)	Do
0	0.08	0.00516	0.05	0.92	0.92	12.9	1.01	0.005
1	0.08	0.00516	0.05	0.92	0.92	12.9	1.01	0.005
2	0.08	0.00516	0.05	0.92	0.92	12.9	1.01	0.005
3	0.08	0.00516	0.05	0.92	0.92	12.9	1.01	0.005

Location #	alpha	z (2/3 H)	T1	G_bar	Wz	H/D	Vd(5/6H)	Kz(5/6H)
0	7	72.2	0.147	1.232		117.72	136.6	1.34
1	7	72.2	0.147	1.232	220.06	117.72	136.6	1.34
2	7	72.2	0.147	1.232	270.27	117.72	136.6	1.34
3	7	72.2	0.147	1.232	303.39	117.72	136.6	1.34

Location #	Cf	D_min(qz)^.
0	0.6158	
1	0.6158	4.724
2	0.6158	5.235
3	0.6158	5.55

The above hand calculations were used to check STACK1. An option within the code allows the user to view all of the above variables used in the calculations.

Appendix 2: Derivation of Tapered Transfer Matrix

A.2.1 Derivation of the transfer matrix from an *n*th-order differential equation

In order to obtain the transfer matrix for the flexural vibrations of a tapered beam, a characteristic equation representing this beam needs be derived first. Drawing from the methods described in Pestel and Leckie [50],

> "The usual method of solving problems of one independent variable is to eliminate *n*-1 of the dependent variables to give an *n*th-order ordinary differential equation in the remaining dependent variable. If it is possible to find *n* closed solutions of this equation, it is then a straightforward matter to develop the transfer matrix. The *n* constants associated with the *n*th-order differential equation are determined by the boundary conditions of the problem. We shall find these constants in terms of the components of the state vector at an arbitrary point *I*-1 of the system."

Therefore, it is necessary to first derive an *n*th order differential equation for the tapered beam, and then find the *n* closed solutions to this equation.

A.2-2 Transfer matrix for the flexural vibrations of a linear tapered beam including the effect of shear deflection and rotary inertia

The transfer matrix for the flexural vibrations of a *constant* beam including the effect of shear deformation and rotary inertia is solved in Pestel and Leckie. In order to take this derivation one step further, the same process will be followed, but with the following terms being treated as functions of axial length, not constant:

Cross sectional area, $A(x)$

Second moment of area about the y axis, $J_y(x)$

Mass per unit length, $\mu(x)$

Radius of gyration about the y axis, $i_y(x)$

Consider a tapered beam of length l, with the previously mentioned properties variable along its length. The slope dw/dx of the beam center line is affected by both the bending moment and shear force in the following ways:

- The bending moment rotates the face through an angle ψ as shown in Figure A.2-1
- The shearing forces turn the centerline to slope dw/dx as shown in Figure A.2-2

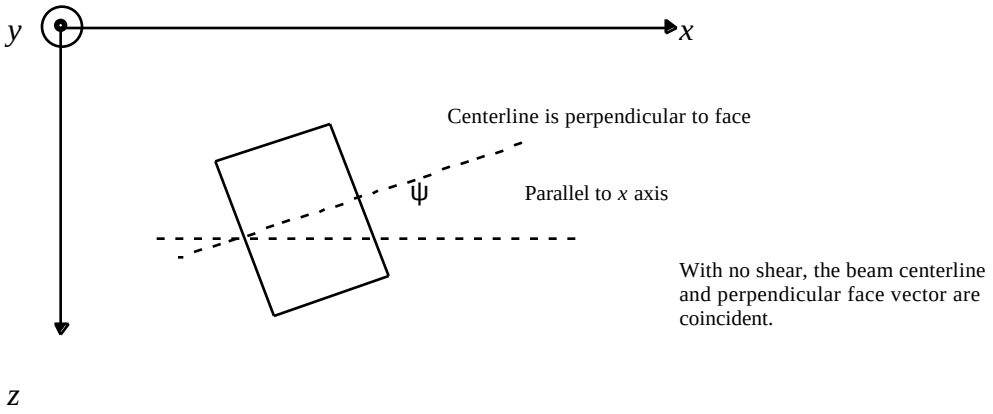

Figure A.2-1. Section of beam acted upon by bending moment only

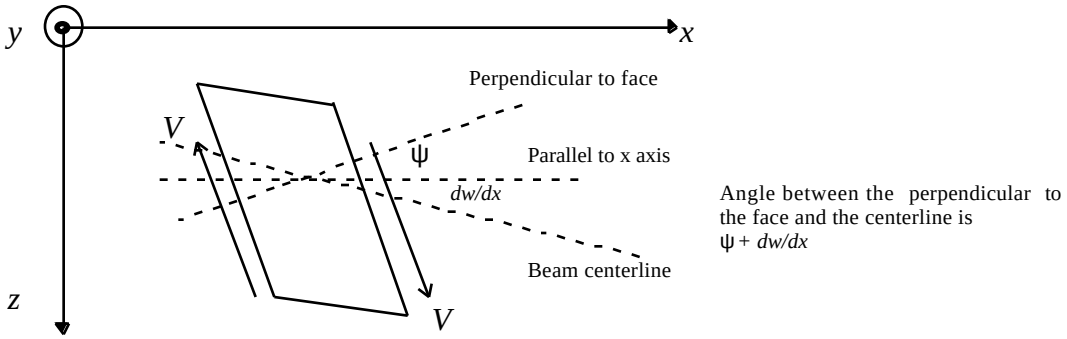

Figure A.2-2. Section of beam acted upon by bending and shear forces

Relationship between the angle ($\psi + dw/dx$) and the shear force V:

$$V = GA_s(dw/dx + \psi) \qquad \text{(A.2.1)}$$

where: $GA_s = GA/k_s = GA(x)/k_s(x)$, k_s = shape factor depending on section shape [51]

The usual bending relation for a beam is:

$$M = EJ_y\, d\psi/dx = EJ_y(x)\, d\psi/dx \qquad \text{(A.2.2)}$$

To derive the equilibrium equations for a beam element, consider the following forces:

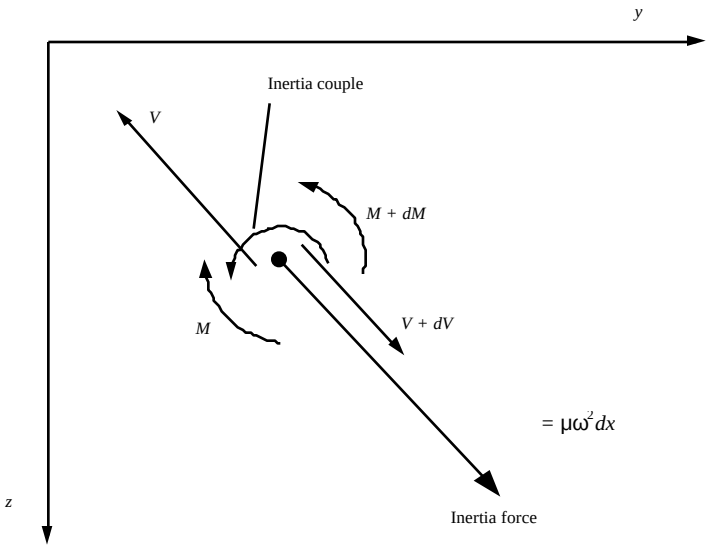

Figure A.2-3. Forces acting on a beam element of length *dx*

Summing the moments about the beam element:

$$(M+dM) - M + [\mu(x) i_y(x)^2 \omega^2 \psi dx] - V dx = 0$$

$$dM = V dx - \mu(x) i_y(x)^2 \omega^2 \psi dx$$

$$dM/dx = V - \mu(x) i_y(x)^2 \omega^2 \psi \qquad \text{(A.2.3)}$$

Summing the forces on the beam element:

$$(V+dV) - V + \mu(x)\omega^2 w(x) dx = 0$$

$$dV/dx = -\mu(x)\omega^2 w(x) \qquad \text{(A.2.4)}$$

Taking the derivative of eqn(A.2.1):

$$\frac{dV}{dx} = \frac{d}{dx}\left[\frac{GA(x)}{K_s(x)}\left(\frac{dw}{dx} + \psi\right)\right] \qquad \text{(A.2.5)}$$

Substituting this expression for *dV/dx* into eqn(A.2.4)

$$\frac{d}{dx}\left[\frac{GA(x)}{K_s(x)}\left(\frac{dw}{dx} + y\right)\right] = -\mu(x)\omega^2 w(x) \qquad \text{(A.2.6)}$$

$$\frac{d}{dx}\left[\frac{GA(x)}{K_s(x)}\left(\frac{d^2w}{dx^2}+\frac{dy}{dx}\right)\right]=-\mu(x)\omega^2 w(x) \qquad \text{(A.2.7)}$$

Substituting in $d\psi/dx$ from eqn(A.2.4):

$$\left[G\frac{d}{dx}\frac{A(x)}{K_s(x)}\left[\frac{d^2w(x)}{dx^2}+\frac{M}{EJ_y(x)}\right]\right]=-\mu(x)\omega^2 w(x) \qquad \text{(A.2.8)}$$

Taking the derivative of eqn(A.2.3):

$$\frac{d^2M}{dx^2}=\frac{dV}{dx}-\frac{d}{dx}\left[\mu(x)i_y(x)^2\omega^2\psi(x)\right]$$

Substitute in for $d\psi/dx$ from eqn(A.2.2) and dV/dx from eqn(A.2.4):

$$\frac{d^2M}{dx^2}=-\mu(x)\omega^2 w(x)-\frac{M}{EJ_y(x)}\left[\frac{d}{dx}\left[\mu(x)i_y(x)^2\omega^2\right]\right] \qquad \text{(A.2.9)}$$

Solving for M in eqn(A.2.5):

$$\frac{d^2w(x)}{dx^2}+\frac{M}{EJ_y(x)}=\frac{-\mu(x)\omega^2 w(x)}{G}\frac{d}{dx}\frac{k_s(x)}{A(x)}$$

$$\frac{M}{EJ_y(x)}=-\frac{d^2w(x)}{dx^2}-\frac{d}{dx}\frac{k_s(x)}{A(x)}\frac{\mu(x)\omega^2 w(x)}{G}$$

$$M = -EJ_y(x)\frac{d^2w(x)}{dx^2} - \frac{d}{dx}\left[k_s(x)\right]\frac{EJ_y(x)\mu(x)\omega^2 w(x)}{G} \qquad \text{(A.2.10)}$$

Substituting this equation for $\boldsymbol{M}$ into eqn(A.2.9):

$$\frac{d^2}{dx^2}\left\{-EJ_y(x)\frac{d^2w(x)}{dx^2} - \frac{d}{dx}\left[k_s(x)\right]\frac{EJ_y(x)\mu(x)\omega^2 w(x)}{G}\right\} = -\mu(x)\omega^2 w(x) - \frac{d}{dx}\left[\mu(x)i_y(x)^2\omega^2\left\{\frac{d^2w(x)}{dx^2} - \frac{d}{dx}\left[k_s(x)\right]\frac{\mu(x)\omega^2 w(x)}{G}\right\}\right]$$

Simplifying this derivative:

$$-E\frac{d^2}{dx^2}\left\{J_y(x)\frac{d^2w(x)}{dx^2}\right\} - \frac{d^2}{dx^2}\left[\frac{d}{dx}\frac{k_s(x)}{A(x)}\right]\frac{EJ_y(x)\mu(x)\omega^2 w(x)}{G} =$$

$$-m(x)\omega^2 w(x) - \frac{d}{dx}\left[\mu(x)i_y(x)^2\omega^2\left\{\frac{d^2w(x)}{dx^2} - \frac{d}{dx}\left[k_s(x)\right]\frac{EJ_y(x)\mu(x)\omega^2 w(x)}{G}\right\}\right] \qquad \text{(A.2.11)}$$

It is from this above equation that the transfer matrix is normally [53]. For a beam with constant cross section, eqn(A.2.11) greatly simplifies to an ordinary differential equation with constant coefficients. However, in order to solve this differential equation, the expressions for $J_y(x)$, $K_x(x)$, $A(x)$, $\mu(x)$, and $i_y(x)$ need to be derived in order to get the equation in terms of only one variable, x. The bending moment for a cylindrical beam is given as:

$$I = \frac{\pi}{64}\left[\left(D_c + T_k^{\,4}\right) - (D_c - T_k)^4\right] \qquad \text{(A.2.12)}$$

where: D_c = Centroidal Diameter, T_k = Wall thickness

For a tapered beam, the centroidal diameter is a function of the axial position, *x*. To derive the bending moment for the following beam, an expression for the taper is needed. The second moment of area of the beam shown in Figure A.2-4 (with taper angle θ and starting radius R_o) can be shown to be:

$$I = \frac{\pi}{64}\left[(2R_o - 2x\tan\theta + T_k)^4 - (2R_o - 2x\tan\theta - T_k)^4\right] \qquad \text{(A.2.12)}$$

Now, the area as a function of *x* [$A(x)$] can be expressed as:

$$A(x) = \pi(R_o - x\tan\theta + t)^2 - \pi(R_o - x\tan\theta)^2$$

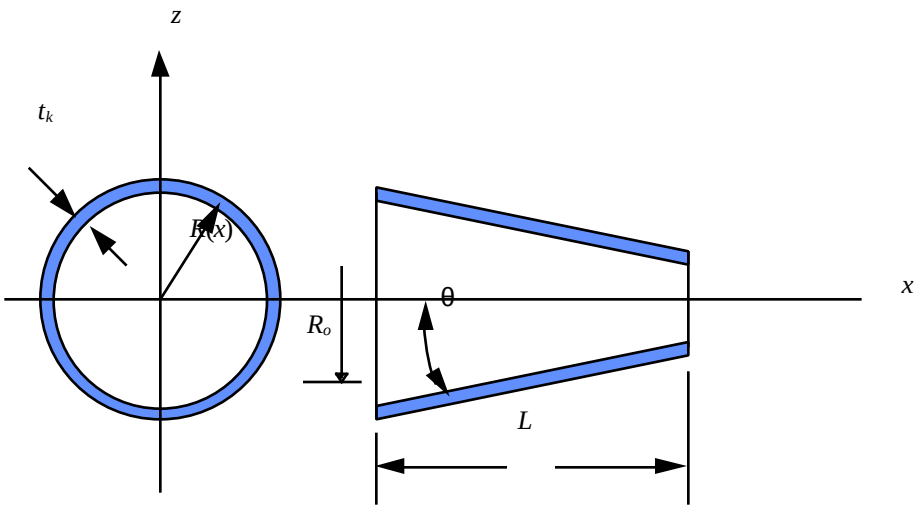

Figure A.2-4. Tapered beam

Mass per unit length, $\mu(x)$ is expressed as:

$$\mu(x) = A(x)\rho = \rho\pi(R_o - x\tan\theta + t)^2 - \pi(R_o - x\tan\theta)^2 \qquad \text{(A.2.13)}$$

The radius of gyration as a function of length, $i_y(x)$ about the y axis is expressed as:

$$i_y^2 = \frac{I_x}{A} = \frac{\frac{\pi}{64}\left[(2R_o - 2x\tan\theta + T_k)^4 - (2R_o - 2x\tan\theta - T_k)^4\right]}{\pi(R_o - x\tan\theta + t)^2 - \pi(R_o - x\tan\theta)^2}$$

Letting $\alpha = R_o - x\tan\theta$,

$$i_y^2 = \frac{I_x}{A} = \frac{\frac{\pi}{64}\left[(2\alpha + T_k)^4 - (2\alpha - T_k)^4\right]}{\pi(\alpha + t)^2 - \pi(\alpha)^2}$$

When substituting the values for $J_y(x)$, $K_x(x)$, $A(x)$, $\mu(x)$, and $i_y(x)$ back into the differential equation of the beam, eqn(A.2.11), high orders of x are encountered, along with extremely large amounts of differentiation and algebra. This task was attempted on the symbolic processors, contained within the software packages MATHEMATICA® and MATLAB®, but the size of the resulting equations grew beyond the capability of the

processor. Due to these difficulties, a closed-form solution of eqn(A.2.11) could not be achieved by normal means.

It is for these reasons that the continuously tapered beam transfer matrix was not implemented, and instead was approximated by a series of stepped beam segments. This approach is shown in Chapter 5 to provide extremely accurate results.

Vita

Joseph Charles Servaites was born on May 22, 1972 in Dayton, Ohio, USA. After graduating from high school in 1990, he enrolled in the University of Cincinnati, Ohio, where he received a Bachelors of Science degree in Mechanical Engineering in 1995. While obtaining this degree he was employed as a co-op at G. E. Aircraft Engines in Cincinnati, Ohio. In Fall of 1995 he enrolled in Virginia Polytechnic and State University in Blacksburg, Virginia where he completed his Masters of Science degree in September, 1996. He plans to start work with G. E. Aircraft Engines in October, 1996. His research was sponsored by the DuPont company.